



**HAL**  
open science

# A root-knot nematode effector Mi2G02 hijacks a host plant trihelix transcription factor for nematode parasitism

Jianlong Zhao, Kaiwei Huang, Rui Liu, Yuqing Lai, Pierre Abad, Bruno Favery, Heng Jian, Jian Ling, Yan Li, Yuhong Yang, et al.

## ► To cite this version:

Jianlong Zhao, Kaiwei Huang, Rui Liu, Yuqing Lai, Pierre Abad, et al.. A root-knot nematode effector Mi2G02 hijacks a host plant trihelix transcription factor for nematode parasitism. *Plant Communications*, 2023, pp.100723. 10.1016/j.xplc.2023.100723 . hal-04221995

**HAL Id: hal-04221995**

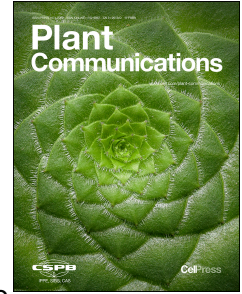
**<https://hal.inrae.fr/hal-04221995>**

Submitted on 29 Sep 2023

**HAL** is a multi-disciplinary open access archive for the deposit and dissemination of scientific research documents, whether they are published or not. The documents may come from teaching and research institutions in France or abroad, or from public or private research centers.

L'archive ouverte pluridisciplinaire **HAL**, est destinée au dépôt et à la diffusion de documents scientifiques de niveau recherche, publiés ou non, émanant des établissements d'enseignement et de recherche français ou étrangers, des laboratoires publics ou privés.

# Journal Pre-proof



A root-knot nematode effector Mi2G02 hijacks a host plant trihelix transcription factor for nematode parasitism

Jianlong Zhao, Kaiwei Huang, Rui Liu, Yuqing Lai, Pierre Abad, Bruno Favery, Heng Jian, Jian Ling, Yan Li, Yuhong Yang, Bingyan Xie, Michaël Quentin, Zhenchuan Mao

PII: S2590-3462(23)00269-9

DOI: <https://doi.org/10.1016/j.xplc.2023.100723>

Reference: XPLC 100723

To appear in: *PLANT COMMUNICATIONS*

Received Date: 3 July 2023

Revised Date: 12 August 2023

Accepted Date: 19 September 2023

Please cite this article as: Zhao, J., Huang, K., Liu, R., Lai, Y., Abad, P., Favery, B., Jian, H., Ling, J., Li, Y., Yang, Y., Xie, B., Quentin, M., Mao, Z., A root-knot nematode effector Mi2G02 hijacks a host plant trihelix transcription factor for nematode parasitism, *PLANT COMMUNICATIONS* (2023), doi: <https://doi.org/10.1016/j.xplc.2023.100723>.

This is a PDF file of an article that has undergone enhancements after acceptance, such as the addition of a cover page and metadata, and formatting for readability, but it is not yet the definitive version of record. This version will undergo additional copyediting, typesetting and review before it is published in its final form, but we are providing this version to give early visibility of the article. Please note that, during the production process, errors may be discovered which could affect the content, and all legal disclaimers that apply to the journal pertain.

© 2023 The Author(s).

1 **A root-knot nematode effector Mi2G02 hijacks a host plant trihelix**  
2 **transcription factor for nematode parasitism**

3 Jianlong Zhao<sup>1,4,\*</sup>, Kaiwei Huang<sup>1,4</sup>, Rui Liu<sup>1,4</sup>, Yuqing Lai<sup>1</sup>, Pierre Abad<sup>2</sup>, Bruno  
4 Favery<sup>2</sup>, Heng Jian<sup>3</sup>, Jian Ling<sup>1</sup>, Yan Li<sup>1</sup>, Yuhong Yang<sup>1</sup>, Bingyan Xie<sup>1</sup>, Michaël  
5 Quentin<sup>2,\*</sup> and Zhenchuan Mao<sup>1,\*</sup>

6 <sup>1</sup> State Key Laboratory of Vegetable Biobreeding, Institute of Vegetables and  
7 Flowers, Chinese Academy of Agricultural Sciences, 100081, Beijing, China

8 <sup>2</sup> INRAE, Université Côte d'Azur, CNRS, ISA, F-06903, Sophia Antipolis, France

9 <sup>3</sup> Department of Plant Pathology and Key Laboratory of Pest Monitoring and Green  
10 Management of the Ministry of Agriculture, China Agricultural University, 100193,  
11 Beijing, China

12 <sup>4</sup> These authors contributed equally: Jianlong Zhao, Kaiwei Huang, Rui Liu.

13 \* **Corresponding:** Email: Jianlong Zhao ([zhaojianlong@caas.cn](mailto:zhaojianlong@caas.cn)), Michaël Quentin  
14 ([michael.quentin@inrae.fr](mailto:michael.quentin@inrae.fr)), Zhenchuan Mao ([maozhenchuan@caas.cn](mailto:maozhenchuan@caas.cn)).

15 **Running title**

16 Mi2G02 effector stabilizes a transcription factor

17 **Short summary**

18 Root-knot nematodes establish parasitic relationships with host plants through  
19 secreting effectors. In this study, we highlight the role of Mi2G02 effector and its  
20 target GT-3a, a trihelix transcription factor, in plant nucleus. Mi2G02 maintains GT-  
21 3a protein stabilization by inhibiting the 26S proteasome-dependent pathway,  
22 leading to a suppression of *TOZ* and *RAD23C* expression, promoting *Meloidogyne*  
23 *incognita* parasitism.

24 **ABSTRACT**

25 Root-knot nematodes (RKNs) cause huge agricultural losses every year. They  
26 secrete a repertoire of effectors to facilitate parasitism through the induction of plant-  
27 derived giant feeding cells, which serve as their sole source of nutrients. However,  
28 the mode of action of these effectors and host targeted proteins remain largely  
29 unknown. In this study, we investigated the role of the effector Mi2G02 in

30 *Meloidogyne incognita* parasitism. Host-derived *Mi2G02* RNA interference in  
31 *Arabidopsis thaliana* affects giant cells development, whereas the ectopic expression  
32 of *Mi2G02* promotes root growth and increases plant susceptibility to *M. incognita*.  
33 We used various combinations of approaches to study the specific interactions  
34 between *Mi2G02* and *A. thaliana* *GT-3a*, a trihelix transcription factor. *GT-3a*  
35 knockout in *A. thaliana* affected feeding site development, resulting in the production  
36 of fewer egg masses, whereas *GT-3a* overexpression in *A. thaliana* increased  
37 susceptibility to *M. incognita* and also root growth. Moreover, we highlight the role of  
38 *Mi2G02* in maintaining *GT-3a* protein stabilization by inhibiting the 26S proteasome-  
39 dependent pathway, leading to a suppression of *TOZ* and *RAD23C* expression,  
40 promoting nematodes parasitism. Thus, this work enhances our understanding of the  
41 manipulation of the role and regulation of a transcription factor by a pathogen  
42 effector through interfering proteolysis pathway to reprogram genes expression for  
43 nematode feeding cells development.

44 **Keywords:** *Meloidogyne incognita*, effector, giant cell, *Mi2G02*, transcription factor,  
45 interaction

## 46 INTRODUCTION

47 Root-knot nematodes (RKNs; *Meloidogyne* spp.) can infect thousands of plant species,  
48 causing huge agricultural losses every year (Abad et al., 2008; Jones et al., 2013).  
49 RKN juveniles induce the redifferentiation of plant vascular cells to establish feeding  
50 structures that support their development into reproductive adult females (Bartlem et  
51 al., 2014). The second-stage juveniles (J2s) enter the host in the root elongation area  
52 and migrate intercellularly toward the vascular tissues, where they select five to seven  
53 parenchyma cells, into which they inject esophageal gland secretions through a  
54 syringe-like stylet (Favery et al., 2020). These secretions contain proteinaceous  
55 effectors, which reprogram the root cells to become giant cells (GCs), hypertrophied  
56 multinucleate feeding cells that undergo several rounds of nuclear division without cell  
57 division and extensive endoreduplication, with expansion by isotropic growth (Caillaud  
58 et al., 2008). The cells surrounding the GCs simultaneously divide, to form a typical  
59 root-knot or gall. The vascular tissues undergo extensive reorganization, and the  
60 xylem proliferates (Baldacci-Cresp et al., 2020; Bartlem et al., 2014; Yamaguchi et al.,  
61 2017). GCs are the only source of nutrients for RKNs throughout their live cycle; the

62 nematode must, therefore, maintain this parasitic interaction for several weeks, until  
63 the female can lay her eggs in a gelatinous matrix on the outside of the root tissues  
64 (Favery et al., 2020).

65 This intricate biotrophic interaction requires the nematode to cope with host  
66 defense responses, to alter host-cell morphology and to hijack the physiology of host  
67 cells for its own benefit. The nematode achieves these ends by inducing a deep  
68 transcriptional reprogramming of host cells, as demonstrated by a large number of  
69 transcriptomic studies (Barcala et al., 2010; Cabrera et al., 2014; Escobar et al., 2011;  
70 Fuller et al., 2007; Jammes et al., 2005; Olmo et al., 2017; Portillo et al., 2009;  
71 Przybylska and Spychalski, 2021; Sato et al., 2021; Shukla et al., 2018; Warmerdam  
72 et al., 2018; Yamaguchi et al., 2017; Zhu et al., 2022). Genes encoding transcription  
73 factors (TFs), which regulate key expression by binding to appropriate DNA elements  
74 and recruiting additional proteins to initiate transcription (Strader et al., 2022), are  
75 among the genes known to display differential expression in galls (Cabrera et al.,  
76 2014; Przybylska and Spychalski, 2021; Yamaguchi et al., 2017; Zhu et al., 2022).  
77 Many of these plant TFs are known to be key players in the regulation of plant  
78 developmental processes and stress responses. They include ETHYLENE-  
79 RESPONSIVE FACTORS (ERF), NO APICAL MERISTEM (NAC), AUXIN  
80 RESPONSE FACTORS (ARF) and LATERAL ORGAN BOUNDARIES DOMAIN-(LBD)  
81 (Shukla et al., 2018). However, very little is known about the role of these TFs in GC  
82 formation and RKNs parasitism. For LBD16, inactivation led to a decrease in infection  
83 or even a total absence of feeding site formation (Cabrera et al., 2014; Olmo et al.,  
84 2017).

85 RKN effectors are clearly involved in modulating host transcriptional responses.  
86 They may act as transcription factors, as has been shown for the *M. incognita* effector  
87 7H08, which localizes to the plant cell nucleus and functions as a transcriptional  
88 activator (Zhang et al., 2015). Other effectors may associate with and dysregulate host  
89 transcription factors. Mi16D10 may be one such effector, as it has been shown to  
90 interact with plant SCARECROW-like transcription factors known to regulate root  
91 development (Huang et al., 2006). Another example is provided by MiEFF18, an  
92 effector that interacts with the spliceosomal protein SmD1 to trigger alternative splicing  
93 events during pre-mRNA maturation in galls, thereby increasing the diversity of host  
94 transcripts (Mejias et al., 2021; Mejias et al., 2022).

95 *M. incognita* secreted protein 2 (*Mi-msp2* or *Mi2G02*) was initially identified as a  
96 putative parasitism gene expressed exclusively in the subventral esophageal gland  
97 cells of parasitic J2s (Huang et al., 2003). It was subsequently shown to be required  
98 for *M. incognita* parasitism in host-derived RNA interference experiments (Joshi et al.,  
99 2022; Joshi et al., 2019). *Mj2G02*, an ortholog from *M. javanica*, has been shown to  
100 suppress Gpa2/RBP-1-triggered cell death in *Nicotiana benthamiana* and jasmonate-  
101 mediated plant immune responses (Song et al., 2021). 2G02 proteins are nuclear  
102 effectors; they have a ShK toxin (ShKT) domain encoding a potassium channel  
103 inhibitor first identified in a sea anemone (*Stichodactyla helianthus*) (Tudor et al., 1996).  
104 Proteins containing ShKT domains are widely expressed in parasitic and non-parasitic  
105 nematodes (Hewitson et al., 2013). There is evidence to suggest that ShkT-like  
106 domains act as contact surfaces for protein interactions (Thein et al., 2009) and for  
107 immune evasion (Chhabra et al., 2014; Niu et al., 2016; Song et al., 2021). However,  
108 the plant target proteins by *Mi2G02* are unknown.

109 In this study, we show that the *Mi2G02* effector interacts with an *Arabidopsis*  
110 *thaliana* trihelix transcription factor, GT-3a, and that this interaction is important for  
111 nematode parasitism. We also demonstrate that GT-3a functions as a transcription  
112 inhibitor, binding to the promoters of *TOZ* and *RAD23C*, thereby modulating plant cell  
113 development for *M. incognita* parasitism. We found that *Mi2G02* stabilized GT-3a by  
114 inhibiting the 26S proteasome-dependent pathway, thereby causing a stronger  
115 suppression of *TOZ* and *RAD23C* expression. Collectively, these results demonstrate  
116 the involvement of a *M. incognita* effector (*Mi2G02*), a plant transcription factor (GT-  
117 3a), and downstream regulatory genes in the formation and development of  
118 multinucleate GCs for nematode parasitism.

## 119 RESULTS

### 120 ***Mi2G02* is a nematode nuclear effector essential for giant cell development**

121 *Mi2G02/MiMSP2* gene encodes a 210-amino acid (aa) protein with an 18 aa N-  
122 terminal signal peptide (SP), a ShK toxin (ShKT) domain (33–69 amino acids) and two  
123 nuclear localization signals (NLS-1 and NLS-2), one of which is located in the ShKT  
124 domain (Figure 1A). Transient expression assays were performed in *Nicotiana*  
125 *benthamiana* leaves, to investigate the functionality of the NLSs *in planta*. *Mi2G02*-  
126 GFP recombinant fusion proteins were detected exclusively in the plant cell nucleus,  
127 exclusively in the nucleoplasm, with exclusion from the nucleolus (Figure 1B). We

128 mutated the two predicted nuclear localization signals in the effector sequence, to  
129 generate Mi2G02-mu1 (mutated NLS-1), Mi2G02-mu2 (mutated NLS-2) and Mi2G02-  
130 mu3 (mutated NLS-1 and NLS-2) (Figure 1A). Mi2G02-mu1-GFP, Mi2G02-mu2-GFP  
131 and Mi2G02-mu3-GFP were found principally in the cytoplasm (Figure 1B).  
132 Immunoblotting using cytoplasmic and nuclear fraction proteins extracted from *N.*  
133 *benthamiana* plant leaves confirmed the nuclear expression of Mi2G02-GFP, but not  
134 Mi2G02-mu1-GFP, Mi2G02-mu2-GFP and Mi2G02-mu3-GFP (Figure 1C). These  
135 results demonstrated the requirement of both NLSs for the localization of Mi2G02 to  
136 the nucleus.

137 We investigated the role of Mi2G02 in giant cell formation, by generating three  
138 homozygous RNAi *A. thaliana* lines expressing the *Mi2G02* hairpin dsRNA. The  
139 expression of the hairpin construct in these RNAi lines was confirmed by PCR  
140 (Supplemental Figure 1A) and the transgenic plants were inoculated with nematodes.  
141 The silencing of *Mi2G02* by host-derived RNAi was validated by RT-qPCR in feeding  
142 nematodes recovered from the infested plants (Figure 2A and Supplemental Figure  
143 1B). Consistent with previous findings (Joshi et al., 2019), *Mi2G02* silencing  
144 decreased the numbers of galls and egg masses by at least 60% in the *Mi2G02* RNAi  
145 lines relative to the two control lines: wild-type plants and a *GFP* RNAi line (Figure 2B  
146 and Supplemental Figure 1B). We investigated the role of Mi2G02 in the formation of  
147 RKN-induced feeding sites further, by analyzing the morphology of the feeding cells  
148 induced in the RNAi lines. All three *Mi2G02* RNAi lines showed significantly smaller  
149 (30%) GC areas than the controls (Figure 2C). These findings suggest that *Mi2G02*  
150 plays a role in nematode parasitism, particularly in the development of GCs.

151 We then generated two transgenic *A. thaliana* lines with ectopic *Mi2G02*  
152 expression. Semiquantitative RT-PCR (Supplemental Figure 2A) and western blot  
153 (Supplemental Figure 2B) were performed to confirm the expression of *Mi2G02* in the  
154 transgenic plants. Interestingly, the roots of the *Mi2G02*-expressing transgenic lines  
155 were 27% and 33% longer ( $n=10$ ) in the two independent lines than those of the wild-  
156 type plants (Figure 2D and Supplemental Figure 3C). In nematode inoculation assays,  
157 both transgenic lines were significantly ( $P < 0.05$ ) more susceptible to *M. incognita*  
158 infection than wild-type plants; the *Mi2G02*-expressing lines had up to 30% more galls  
159 and egg masses than the wild-type plants at 35 dpi (Figure 2E and Supplemental  
160 Figure 2D). Mi2G02 is, therefore, an effector essential for *M. incognita* parasitism, and  
161 able to modulate root growth.

**Mi2G02 interacts with the trihelix transcription factor GT-3a**

We used a yeast two-hybrid (Y2H) screen to identify the proteins of *A. thaliana* targeted by Mi2G02. We used a signal peptide-deficient Mi2G02 as a bait to screen a cDNA library from *M. incognita*-infected *A. thaliana* roots. We identified 20 candidate target proteins, including six proteins annotated as predicted nuclear proteins in TAIR (Supplemental Table 1). Based on the number of captures, and predicted subcellular distributions and functions, we selected three candidate targets for further study: a trihelix transcription factor (GT-3a, AT5G01380), the LATERAL ORGAN BOUNDARIES DOMAIN PROTEIN 41 (LBD41, AT3G020550) and UBIQUITIN EXTENSION PROTEIN 1 (UBQ1, AT3G52990). A pairwise Y2H assay was performed to validate the interactions between Mi2G02 and the full-length GT-3a, LBD41 and UBQ1 proteins. GT-3a was the only protein found to interact with Mi2G02 (Figure 3A and 3B). LBD41 displayed strong auto-activation in yeast, and it was not possible to confirm any interaction between Mi2G02 and UBQ1 (Supplemental Figure 3A).

We investigated the possible involvement of the ShKT domain of Mi2G02 and the DNA-binding domain (DB) of GT-3a in the interaction, by generating two truncated versions of Mi2G02 (Mi2G02-ShKT and Mi2G02- $\Delta$ ShKT) and two truncated versions of GT-3a (GT-3a-DB and GT-3a- $\Delta$ DB) (Figure 3A). Subcellular localization results showed that Mi2G02-ShKT-GFP was localized mainly in the cell nucleus (Supplemental Figure 3B). Pairwise Y2H experiments demonstrated that the ShKT domain of Mi2G02 and the DB domain of GT-3a were required for the interaction between these two proteins (Figure 3B). We also investigated the requirement of the NLSs of Mi2G02 for the interaction with GT-3a in yeast. Pairwise Y2H experiments with Mi2G02-mu1, Mi2G02-mu2 and Mi2G02-mu3 showed that both the NLSs of Mi2G02 were required for interaction with GT-3a (Figure 3C).

The co-expression of Mi2G02-GFP and mcherry-GT-3a in *N. benthamiana* leaf cells showed that the effector and its target were colocalized in the nucleoplasm of the plant cells (Figure 3D). We then investigated the interactions between Mi2G02 and GT-3a *in planta*, by performing bimolecular fluorescence complementation (BiFC) assays. The co-expression of Mi2G02 fused to the N-terminal part of YFP (Mi2G02-nEYFP) and GT-3a fused to the C-terminal part of YFP (GT-3a-cEYFP) in *N. benthamiana* epidermal leaf cells resulted in a reconstitution of YFP activity in the plant cell nucleus, whereas no YFP fluorescence was observed if Mi2G02 with mutated NLSs or an empty vector was used (Figure 3E and Supplemental Figure 3C).



196 A split luciferase complementation assay (LCA) and a co-immunoprecipitation  
197 (Co-IP) assay were performed for further verification of the interaction between  
198 Mi2G02 and GT-3a *in planta*. A positive luciferase signal was obtained when Mi2G02  
199 was co-expressed with GT-3a in *N. benthamiana* leaves, as luciferase activity was  
200 reconstituted by the interaction between Mi2G02 and GT-3a, whereas no luciferase  
201 signal was observed if Mi2G02 with mutated NLSs or the GUS control was used  
202 (Figure 3F). In the Co-IP assay, Mi2G02-HA, HA empty vector or GFP-HA and GT-3a-  
203 GFP were co-expressed in *N. benthamiana* leaves. GT-3a-GFP coprecipitated with  
204 Mi2G02-HA but not with Mi2G02-mu1-HA, Mi2G02-mu2-HA and Mi2G02-mu3-HA  
205 (Figure 3G). There is, therefore, a direct interaction between the nuclear Mi2G02 and  
206 *A. thaliana* GT-3a TF *in planta*.

### 207 **GT-3a is important for *M. incognita* parasitism**

208 GT-3a has been reported to be predominantly expressed in floral buds and roots,  
209 especially at the onset of secondary root development (Ayadi et al., 2004). RNA-seq  
210 data for *M. incognita*-infected *A. thaliana* galls at 3, 5 and 7 days post inoculation (dpi)  
211 and for non-infected roots showed that *GT-3a* was significantly upregulated by  
212 nematode infection at these early time points (Yamaguchi et al., 2017). For the  
213 analysis of *GT-3a* expression in galls, we cloned a fragment of the GT-3a promoter (-  
214 2023 to 0) and transformed *A. thaliana* plants with a *ProGT-3a:GUS* fusion. We then  
215 inoculated the transformed plants with *M. incognita* and performed histochemical  
216 assays. We observed a strong GUS signal in uninfected root vascular tissues and  
217 lateral root initials, and in developing galls at 3, 5 and 7 dpi (Figure 4A). These results  
218 suggest that *GT-3a* plays a role early in nematode feeding site development.

219 We explored the biological functions of GT-3a during gall formation in two *gt-3a*  
220 T-DNA knockout (KO) mutant *A. thaliana* lines (*SALK\_134703* and *SALK\_040448*)  
221 (Supplemental Figure 4A). We also generated transgenic *A. thaliana* lines  
222 overexpressing a GT-3a-GFP fusion and GFP alone. Homozygous KO mutants were  
223 verified by PCR and semiquantitative RT-PCR (Supplemental Figure 4B and 4C). Two  
224 independent *GT-3a-GFP*-overexpressing lines were selected and verified by  
225 semiquantitative RT-PCR, western blotting and observing GFP fluorescence  
226 (Supplemental Figure 5D-5F). No macroscopic root phenotype was observed in the  
227 two *gt-3a* T-DNA KO lines relative to wild-type Col-0 (Supplemental Figure 4G). As  
228 observed for Mi2G02, the two independent *GT-3a-GFP*-overexpressing lines had  
229 longer roots (8%;  $n=10$ ) than the wild-type plants, and also had a larger number (92%

230 and 87%;  $n=10$ ) of lateral roots and a greater lateral root density than the wild-type  
231 plants (Figure 4B and 4C and Supplemental Figure 4H). These lines were then  
232 subjected to nematode infection assays. *GT-3a*-overexpressing plants had larger  
233 numbers of galls and egg masses (37% and 48%,  $n=18$ ) than control plants (Figure  
234 4D and Supplemental Figure 5A). By contrast, the two *gt-3a* mutants were significantly  
235 less susceptible to *M. incognita* than control plants, as shown by their smaller numbers  
236 of galls (more than 60% fewer,  $n=26$ ) and the almost complete absence of egg  
237 masses (Figure 4E and Supplemental Figure 5B). In these KO lines, the areas  
238 covered by GCs were 40% ( $n=10$ ) smaller than those in control plants (Figure 4F).  
239 The *GT-3a* transcription factor, therefore, regulates root development and plays an  
240 essential role in GC development and *M. incognita* parasitism.

#### 241 ***GT-3a* targets and represses *TOZ* and *RAD23C***

242 We investigated the transcriptional activity of *GT-3a*, by fusing the *GT-3a* coding  
243 sequence to the sequence encoding the GAL4 DNA-binding domain in the pGBKT7  
244 (BD) vector, and using the resulting plasmid to transform the yeast strain AH109.  
245 Yeast cells transformed with the positive control pCL-1, encoding the full-length wild-  
246 type GAL4 protein, grew well on SD-Trp-His selection medium and displayed X- $\alpha$ -Gal  
247 activity (Figure 5A). By contrast, yeast cells harboring BD-*GT-3a* or the empty BD  
248 plasmid (negative control) were unable to grow on SD-Trp-His selection medium  
249 (Figure 5A). These results suggest that *GT-3a* does not act as a transcriptional  
250 activator and, therefore, probably acts by repressing gene expression.

251 We then sought to identify the genes for which expression was modulated by *GT-*  
252 *3a*, by searching *A. thaliana* promoter sequences for 5'-GTTAC-3' DNA element,  
253 which was known to be specifically targeted by *GT-3a* (Ayadi et al., 2004), and for the  
254 5'-CACGTG-3' DNA element, with the PlantRegMap tool (Tian et al., 2019). Further,  
255 we turned to the ePlant online tools and explored the expression patterns of candidate  
256 genes under nematode infection and in developing roots (Waese et al., 2017). We  
257 retrieved nine putative *GT-3a* targets (Supplemental Table 2), which were then further  
258 studied with a yeast one-hybrid (Y1H) approach. The Y1H assay revealed that *GT-3a*  
259 bound directly to the promoters of *TORMOZ* (*TOZ*; *AT5G16750*), *RADIATION*  
260 *SENSITIVE 23C* (*RAD23C*; *AT3G02540*) and a WRKY transcription factor (*WRKY2*;  
261 *AT5G56270*) (Figure 5B and Supplemental Figure 6).

262 We investigated the ability of *GT-3a* to repress the expression of *TOZ*, *RAD23C*  
263 or *WRKY2* in a dual-luciferase reporter assay. A construct expressing *GT-3a* and a

264 reporter construct consisting of the *TOZ*, *RAD23C* or *WRKY2* promoter driving  
265 transcription of the firefly luciferase (*LUC*) reporter gene were used for the co-  
266 infiltration of *N. benthamiana* leaves. *GT-3a* decreased the activity of the *TOZ* and  
267 *RAD23C* promoters, measured as a *firefly-to-Renilla* (LUC/REN) luciferase ratio, by  
268 30% and 50%, respectively, relative to the GFP control, whereas it did not decrease  
269 *WRKY2* promoter activity (Figure 5C). For confirmation of this result, we used RT-  
270 qPCR to quantify *TOZ* and *RAD23c* expression in transgenic *A. thaliana* plants  
271 overexpressing *GT-3a*. Both *TOZ* and *RAD23c* appeared to be repressed in the two  
272 independent transgenic lines relative to the wild type (Figure 5D).

273 Finally, we produced a recombinant *GT-3a* protein, which was used in a gel  
274 electrophoretic mobility shift assay (EMSA). *GT-3a-His* significantly decreased the  
275 electrophoretic mobility of the *TOZ* and *RAD23C* promoter probes containing GTTAC  
276 or CACGTG elements, but had no effect on the mobility of the mutated probes (GTTAC  
277 replaced by AAAAA, CACGTG replaced by AAAAAA) (Figure 5E). This result validates  
278 the binding of *GT-3a* to the *TOZ* and *RAD23c* promoters, and indicates that both the  
279 GTTAC and CACGTG elements are important for binding.

280 These results confirm that *GT-3a* can bind the *TOZ* and *RAD23C* promoters  
281 specifically, downregulating the expression of genes driven by these promoters.

### 282 **Mi2G02 promotes *GT-3a* function by stabilizing protein level for nematode** 283 **parasitism**

284 The *toz* mutant is not viable at postembryonic stages (Griffith et al., 2007) and could  
285 not, therefore, be tested in interaction with the nematode. We investigated the role of  
286 *RAD23C* in the plant response to *M. incognita* parasitism, with a *rad23c* T-DNA KO  
287 mutant *A. thaliana* line (*SALK\_068091*) obtained from ABRC (Supplemental Figure  
288 7A). Homozygous KO plants were verified by PCR on genomic DNA (Supplemental  
289 Figure 7B) and by RT-qPCR on cDNA (Supplemental Figure 7C). No difference in root  
290 phenotype was observed between the *rad23c* T-DNA KO line and wild-type plants  
291 (Supplemental Figure 7D), consistent with previous reports (Farmer et al., 2010).  
292 Following *M. incognita* infection, the *rad23c* KO lines were significantly more  
293 susceptible to the nematode than control plants, as shown by the larger numbers of  
294 galls (43%,  $n=28$ ), and egg masses (39%) observed (Figure 6A and Supplemental  
295 Figure 7E). *RAD23C* therefore downregulates *M. incognita* parasitism.

296 We addressed the potential outcome of Mi2G02 binding to *GT-3a* more precisely,  
297 by co-expressing Mi2G02 and *GT-3a* in *N. benthamiana* leaves and performing dual-

298 luciferase reporter assays. The previously observed suppression of *TOZ* and *RAD23C*  
299 expression mediated by GT-3a was significantly enhanced in the presence of Mi2G02  
300 (Figure 6B). We also performed transient expression assays and western blotting to  
301 determine whether Mi2G02 affected the amount of GT-3a protein in *N. benthamiana*  
302 agro-infiltrated leaves. The co-expression of Mi2G02 and GT-3a-GFP in *N.*  
303 *benthamiana* leaves resulted in a significant higher GFP fluorescence intensity (500%  
304 to 660% higher) compared with the controls using mutant Mi2G02 or MiEFF18 (Figure  
305 6C and Supplemental Figure 8). Similarly, the co-expression of Mi2G02 and GT-3a in  
306 *N. benthamiana* leaves resulted in high levels of GT-3a protein accumulation. No such  
307 accumulation was observed with empty vector, Mi2G02 mutants or MiEFF18, used as  
308 negative controls (Figure 6D and 6E). Furthermore, treatment with a proteasome  
309 inhibitor, MG132, inhibited the degradation of GT-3a (Figure 6E), suggesting that  
310 Mi2G02 stabilized GT-3a protein level by inhibiting the 26S proteasome-dependent  
311 pathway. Together, these results suggest that the Mi2G02 effector helps to stabilize  
312 the GT-3a protein, enabling GT-3a to repress the target genes *TOZ* and *RAD23C*, to  
313 promote nematode parasitism (Figure 7).

## 314 DISCUSSION

315 Phytopathogen success depends on the secretion of effector proteins to reprogram  
316 the host transcriptome to facilitate parasitism. Pathogens have been shown to secrete  
317 effectors that can function as TFs or target TFs to manipulate host cell physiology  
318 and/or immunity. In plant-nematode interactions, the 10A07 effector from the sugar  
319 beet cyst nematode, *Heterodera schachtii*, is expressed in the nematode dorsal gland  
320 cell and targets a plant kinase and the IAA16 transcription factor. There is also  
321 evidence to suggest that the 10A07-IAA16 interaction interferes with auxin signaling  
322 by modulating the expression of several auxin response factors (Hewezi et al., 2015).  
323 Nevertheless, the function of nematode nuclear effectors and the ways in which they  
324 manipulate their host targets for feeding site initiation and development remain largely  
325 elusive. In this study, we characterized the function of a nuclear effector protein,  
326 Mi2G02, and identified its plant target for giant cell formation, the nuclear trihelix  
327 transcription factor GT-3a.

328 Trihelix transcription factors (GTs) are unique to plants and have been shown to  
329 be involved in embryogenesis and subsequent plant growth and development and in  
330 abiotic stresses (Kaplan-Levy et al., 2012). The *A. thaliana* *AtGT-3b* and the maize

331 (*Zea mays*) *ZmGT-3b*, of the GT-1 clade, are induced by pathogens (Park et al., 2004;  
332 Zhang et al., 2021). We show here that *Mi2G02* can interact with the *A. thaliana* GT-  
333 1 clade protein *AtGT-3a*, resulting in the stabilization of this protein. *AtGT-3a* is  
334 induced during the development of galls induced by *M. incognita*. Using *A. thaliana*  
335 transgenic plants in which *AtGT-3a* expression was suppressed or constitutively  
336 induced, we demonstrated that *AtGT-3a* was important for giant cell development and  
337 successful RKN parasitism.

338 The *de novo* formation of new organs, such as lateral roots, rhizobium-induced  
339 nodules or nematode-induced galls from one or a few root cells requires the  
340 recruitment of similar developmental programs (Olmo et al., 2020; Soyano et al., 2019;  
341 Yamaguchi et al., 2017). Several genes, including *ABERRANT LATERAL ROOT*  
342 *FORMATION 4 (ALF4)*, a *RIBULOSE-PHOSPHATE 3-EPIMERASE (RPE)* and  
343 *YUCCA4 (YUC4)*, have been reported to have functions associated with lateral root  
344 initiation and/or development and expression regulated in nematode-induced galls;  
345 they have also been shown to be required for normal feeding site formation and  
346 nematode development (Favery et al., 1998; Olmo et al., 2019; Suzuki et al., 2022).  
347 These genes include cell-cycle genes and TF genes, such as *LBD16* and *PUCHI*, that  
348 play key roles in controlling lateral root initiation and morphogenesis (Torres-Martínez  
349 et al., 2019), and are induced following nematode infection and required for feeding  
350 site development and successful RKN parasitism (Cabrera et al., 2014; Suzuki et al.,  
351 2021). Similarly, *Medicago truncatula* *LBD16* mutants display nodule initiation defects  
352 on inoculation with *Sinorhizobium meliloti* (Schiessl et al., 2019). The rewiring of  
353 transcriptional networks to alter root system architecture also involves changes in  
354 endogenous levels of growth-related plant hormones, and the production of  
355 phytohormones or deployment of hormone-mimicking strategies by symbiotic and  
356 parasitic microbes (Eichmann et al., 2021; Gheysen and Mitchum, 2019). We show  
357 here that the expression of *Mi2G02* in *A. thaliana* can promote root growth and the  
358 development of giant cells, and that *Mi2G02* acts by stabilizing *AtGT-3a*, with  
359 mutations of the gene encoding this transcription factor also impairing giant cell  
360 formation. *AtGT-3a* was found to be strongly induced at the onset of lateral root  
361 development (this study and (Ayadi et al., 2004)). *AtGT-3a* therefore seems to be one  
362 of the TFs regulating both lateral root development and nematode-feeding site neo-  
363 organogenesis.

364 The binding of GT-3a to the promoter of the *TOZ* and *RAD23C* genes was  
365 confirmed by Y1H and EMSA assays. *TOZ* is a predicted WD40 repeat protein  
366 involved in the regulation of cell division planes and the expression of patterning  
367 genes during embryogenesis. It may, therefore be involved in plant embryogenesis  
368 and organogenesis, including root development (Griffith et al., 2007), suggesting a  
369 possible role in the regulation of root-knot neo-organogenesis. *RAD23* probably acts  
370 as a shuttle protein, delivering ubiquitinated substrates to the ubiquitin/26S  
371 proteasome system for degradation. Roles in plant processes as diverse as the cell  
372 cycle, cell morphogenesis, and flower development have been proposed for *RAD23*  
373 (Farmer et al., 2010; Maclean et al., 2014). Interestingly, a role for *RAD23* proteins in  
374 plant immunity has been proposed, probably through interactions with stress-  
375 associated proteins (SAPs) acting as ubiquitin E3 ligases (Kang et al., 2017; Liu et  
376 al., 2019). Consistently, *RAD23* proteins have been shown to be targeted by plant  
377 pathogen effectors, possibly to modulate host protein degradation and suppress host  
378 defense responses. The *A. thaliana* *RAD23A* was identified as a putative target of the  
379 *Pseudomonas syringae* HopM1 effector (Nomura et al., 2006), and the phytoplasma  
380 SAP54 effector was shown to interact with both *RAD23C* and *RAD23D* (Maclean et  
381 al., 2014). Intriguingly, a previous report confirmed that *RAD23* proteins associated  
382 with the 26S proteasome and played an essential role in the cell cycle (Farmer et al.,  
383 2010), roles of *GT-3a* and *RAD23C* in proteolysis and cell fate determination are  
384 expected. In support of this, the transcription activity assays performed in yeast and  
385 *in planta* demonstrated that *GT-3a* downregulated expression of the *TOZ* and  
386 *RAD23C* genes, which suppression was enhanced by co-expressing with *Mi2G02*.  
387 Moreover, *Mi2G02* stabilized *GT-3a* protein level by inhibiting the 26S proteasome-  
388 dependent pathway. Using *rad23c* KO *A. thaliana* lines, we showed that *RAD23C*  
389 inactivation increased susceptibility to RKNs, demonstrating that *RAD23C* is a key  
390 gene for plant-nematode interactions.

391 It has been suggested that *Mj2G02* interferes with both jasmonate signaling and  
392 plant immune responses (Song et al., 2021). *Mj2G02* expression *in planta* resulted in  
393 the accumulation of jasmonoyl-isoleucine, the endogenous bioactive form of  
394 jasmonate (JA), in transgenic *A. thaliana*, and a dysregulation of the expression of  
395 *JASMONATE ZIM DOMAIN (JAZ)* transcriptional repressors and jasmonate-  
396 responsive genes (Song et al., 2021). Our data indicate that *Mi2G02* could divert the  
397 host plant developmental program to promote the formation of the feeding sites

398 important for nematode development and reproduction. RKNs may secrete the 2G02  
399 effector to stabilize GT-3a, maintaining the concentration of this TF at a sufficiently  
400 high level to repress the growth regulator genes, *TOZ* and *RAD23c*, thereby promoting  
401 GC development. We hypothesise that, as previously suggested for ZmGT-3a (Zhang  
402 et al., 2021), GT-3a acts at the interface between growth and immunity. Microbes can  
403 interfere with central regulators of root cell identity and root growth that are also  
404 involved in the response to biotic stress (Rich-Griffin et al., 2020; üstüner et al., 2022).  
405 Plant hormones, the signaling pathways of which may interact at central hubs, also  
406 regulate growth-immunity tradeoffs (Guo et al., 2018; Huot et al., 2014). For instance,  
407 cross-talk between gibberellin (GA)-mediated growth and JA-mediated defense  
408 signaling pathways participates contributes to maintaining the balance between  
409 growth and immunity (Huot et al., 2014; Pieterse et al., 2014). DELLA proteins repress  
410 growth-related TFs unless they are degraded in the presence of growth-promoting  
411 GA. DELLA also binds to JAZs, and DELLA degradation allows JAZs to interact with  
412 their cognate TFs, thereby decreasing JA-dependent signaling. Treatment with flg22  
413 suppresses GA-mediated DELLA degradation, leading to an inhibition of root growth  
414 dependent on salicylic acid (SA), an antagonist of the JA signaling pathway (Huot et  
415 al., 2014; Pieterse et al., 2014). JA is a known growth inhibitor that stabilizes DELLA  
416 and has been shown to downregulate the cyclin-dependent kinases CDKA1 and  
417 CYCB1;1 required for cell-cycle progression (Qi and Zhang, 2020; Reitz et al., 2015).  
418 Biotic stress may, therefore, affect cell cycle regulators, and cell division and  
419 hormones influence the underlying regulatory mechanisms.

420 The plant response to pathogens is highly dependent on the interplay between  
421 immunity and development. Regulators of cell identity and TFs may play a crucial  
422 role in connecting the developmental and immunity gene networks to reflect  
423 response specificity (Rich-Griffin et al., 2020). By modulating GT-3a TF availability in  
424 plant cells, the RKN effector 2G02 can alter both the root developmental program  
425 and JA-dependent signaling pathways to allow giant cell formation and successful  
426 parasitism. In this respect, GT-3a constitutes a novel example of a key regulator  
427 recruited by a biotrophic pathogen at the interface between growth and immunity.

## 428 **METHODS**

### 429 **Nematodes and plant materials**

430 *Meloidogyne incognita* was reproduced on tomato plants (*Solanum lycopersicum* var.  
431 'MoneyMaker'). Egg masses and preparasitic second-stage juveniles (pre-J2s) were  
432 collected as previously described (Zhao et al., 2019). *Arabidopsis thaliana* seeds were  
433 germinated on Murashige and Skoog (MS) medium (Coolaber, Cat. No. PM1012) at  
434 25°C in a growth chamber and the seedlings were transplanted into pots of soil at 13  
435 days. The *gt-3a* T-DNA mutant lines (*SALK\_014703* and *SALK\_040448*), and the  
436 *At3g02540* (*rad23c*) T-DNA mutant line (*SALK\_068091*) were obtained from the  
437 Arabidopsis Biological Resource Center (ABRC, USA). The homozygous plants were  
438 verified by PCR and semiquantitative RT-PCR. *Nicotiana benthamiana* plants and *A.*  
439 *thaliana* plants were grown in pots and placed in a culture room at a temperature of  
440 23°C, with a 16 h light/8 h dark photoperiod, with fluorescent bulbs used to generate  
441 soft white light.

#### 442 **Nematode infections and gall sections**

443 *A. thaliana* seedlings (one month after transplanting) were inoculated with pre-J2s. For  
444 nematode susceptibility assays, *A. thaliana* roots were inoculated with 200 pre-J2s per  
445 plant. The roots were collected and galls and egg masses were counted under a  
446 dissecting microscope (Olympus, Japan) 35 days post inoculation (dpi). For gall  
447 collection, roots were inoculated with 500 pre-J2s per plant. Galls were collected at 3  
448 dpi, 5 dpi, 7 dpi, 14 dpi and 21 dpi and fixed as previously described (Gavrilovic et al.,  
449 2016). At least 10 galls were fixed for each *A. thaliana* line. Gall sections were stained  
450 with 0.05% toluidine blue and photographed on a Zeiss microscope (Zeiss Axiolmager  
451 Z2, Germany). The areas of the giant cells were measured with ImageJ software  
452 (Schindelin et al., 2012). Generally, the first step is to open the program and draw a  
453 line as the same with image scale, then go to 'Analyze', 'Set Scale' and enter the  
454 values: 'known distance' is 100, and 'Unit of length' is 'µm', select 'Global' and click  
455 'OK'. The second step is to go to 'Analyze', 'Set Measurements', select 'Area' and click  
456 'OK'. The third step is to select 'Freehand selections', select giant cell area, go to  
457 'Analyze', select 'Measure' and click 'OK'.

#### 458 **DNA/RNA isolation and gene amplification**

459 *M. incognita* RNA was extracted with TRIzol reagent (Invitrogen, USA, Cat. No.  
460 10296010) as previously described (Lin et al., 2013; Zhao et al., 2021). Total RNA was  
461 extracted from *A. thaliana* seedlings (ten days after germination) with the RNAPrep  
462 Pure Plant Kit (TIANGEN, Cat. No. DP432), according to the manufacturer's  
463 instructions. The RNA was then used for cDNA synthesis with the M-MLV reverse



464 transcriptase (TaKaRa, Cat. No. 2641Q) in accordance with the manufacturer's  
465 instructions. DNA was extracted with the Plant Genomic DNA Kit (TIANGEN, Cat. No.  
466 DP305) according to the manufacturer's instructions. Gene and promoter sequences  
467 were amplified from cDNA or gDNA by PCR with specific primers. All the primers used  
468 in this study are provided in Supplemental Table S3 and were synthesized by TsingKe  
469 Biotechnology Co. Ltd, Beijing, China.

#### 470 **RT-qPCR analysis**

471 RNA was extracted and cDNA was synthesized for reverse transcription-quantitative  
472 PCR (RT-qPCR), with the BIO-RAD CFX96 (BIO-RAD, USA) real-time PCR system,  
473 as follows: 95 °C for 5 min and 40 cycles of 95 °C for 30 s and 60 °C for 30 s. The  
474 data were analyzed with the  $2^{-\Delta\Delta CT}$  method (Livak and Schmittgen, 2001). For internal  
475 controls, *M. incognita* GAPDH (*Minc12412*) or *A. thaliana* UBP22 (*AT5G10790*) was  
476 used for the normalization of RT-qPCR data. RT-qPCR assays were repeated three  
477 times.

#### 478 **Plasmid construction and plant transformation**

479 For RNAi experiments in *A. thaliana*, a 204-nucleotide *Mi2G02* fragment was amplified  
480 and inserted upstream and downstream from the pSAT5 intron in the forward and  
481 reverse orientations (Dafny-Yelin et al., 2007), and then inserted into the pSUPER  
482 destination vector, to construct pSUPER-Mi2G02-RNAi.

483 A signal peptide-deficient *Mi2G02* sequence and ShKT domain were amplified by  
484 PCR and inserted into the Super-GFP (C-terminal GFP) to generate Super-Mi2G02-  
485 GFP and Super-Mi2G02-ShKT-GFP. The nuclear localization sequences of *Mi2G02*  
486 were mutated and inserted into Super-GFP vector to generate Super-Mi2G02-mu1-  
487 GFP, Super-Mi2G02-mu2-GFP and Super-Mi2G02-mu3-GFP. The ORF of *GT-3a* was  
488 inserted into the pBin-mcherry (N-terminal mcherry) vector to generate pBin-mcherry-  
489 *GT-3a*. Plasmids were checked by sequencing and used to transform *A. tumefaciens*  
490 strain GV3101.

491 For ectopic expression in *A. thaliana*, the *Mi2G02* (without signal peptide  
492 sequences) and *AT5G01380* (*GT-3a*) ORFs were amplified and the corresponding  
493 PCR fragments were inserted into the Super-HA vector (C-terminal HA tag) and the  
494 Super-GFP (C-terminal GFP tag) vector to construct Super-Mi2G02-HA and Super-  
495 *GT-3a*-GFP, respectively. The plasmids were verified by sequencing and used to  
496 transform *A. tumefaciens* GV3101, with empty vectors used as a control.

497 For the yeast two-hybrid (Y2H) screens, *Mi2G02* (lacking the signal peptide  
498 sequence) was amplified and inserted into the pGBKT7 (BD) vector. For pairwise Y2H  
499 verification, the coding sequences of *AT5G01380* (*GT-3a*), *AT3G52590* and  
500 *AT3G02550* were inserted into the pGADT7 (AD) vector. For identification of the key  
501 domains for interaction, *Mi2G02-ShKT* (*Mi2G02* retaining the ShKT domain) and  
502 *Mi2G02-ΔShKT* (*Mi2G02* without the ShKT domain) were amplified and inserted into  
503 BD vectors, and *GT-3a-DB* (*GT-3a* retaining the DNA-binding domain) and *GT-3a-  
504 ΔDB* (*GT-3a* lacking the DNA-binding domain) were inserted into AD vectors. The  
505 plasmids were verified by sequencing and used to transform Y2HGold competent  
506 yeast cells.

507 For the yeast one-hybrid (Y1H) assay, the coding region of *GT-3a* was amplified  
508 and inserted into the pB42AD vector. Fragments of candidate promoters were  
509 amplified and inserted into the pLacZi vector.

510 For the bimolecular fluorescence complementation (BiFC) assay, *Mi2G02*  
511 (lacking the signal peptide sequence) and *GT-3a* coding sequences were inserted into  
512 the nE-YFP and cE-YFP vectors (Walter et al., 2004), respectively.

513 For the luciferase complementation assay (LCA), the full-length coding sequence  
514 of *Mi2G02* (lacking the signal peptide sequence) or *GT-3a* was inserted into the  
515 pCAMBIA1300-nLUC or pCAMBIA1300-cLUC vector. The plasmids were verified by  
516 sequencing and used to transform *A. tumefaciens* GV3101.

517 For the co-immunoprecipitation (Co-IP) assay, the coding regions of *Mi2G02*  
518 (lacking the signal peptide sequence) or *GT-3a* were inserted into the super1300  
519 vectors with an HA-tag and a FLAG-tag, respectively, fused to the C-terminal end of  
520 the sequence. Plasmids were verified by sequencing and used to transform *A.  
521 tumefaciens* GV3101.

522 For GUS-staining assays, a 2023 bp fragment of the *GT-3a* promoter was inserted  
523 into the pBI101 vector to generate *ProGT-3a:GUS*. The resulting plasmid was verified  
524 by sequencing and used to transform *A. tumefaciens* GV3101.

525 For dual-luciferase reporter assays, the coding sequence of *GT-3a* was amplified  
526 and inserted into the pCAMBIA3301 vector to generate pCAMBIA3301-*GT-3a*. A 623  
527 bp fragment upstream from the start codon of *TOZ* and a 595 bp fragment upstream  
528 from the start codon of *RAD23C* were amplified and inserted into the pro-LUC-35S-  
529 Rluc vector to generate *TOZpro-LUC-35S-Rluc* and *RAD23Cpro-LUC-35S-Rluc*,

530 respectively. The plasmids were verified by sequencing and used to transform *A.*  
531 *tumefaciens* strain GV3101.

532 A recombinant GT-3a protein was produced by amplifying the coding sequence  
533 of *GT-3a* and inserting it into the pET30a vector (C-terminal His tag) to generate  
534 pET30a-GT-3a. The resulting plasmid was verified by sequencing and used to  
535 transform *Escherichia coli* strain BL21 (DE3) cells.

536 The primers (synthesized by Tsingke Biotechnology Co., Ltd., Beijing, China) and  
537 restriction enzymes (NEB, MA, USA) used for plasmid construction are listed in  
538 Supplemental Table 3.

### 539 **Generation of transgenic *A. thaliana* plants and nematode infection assays**

540 The sequenced pSUPER-Mi2G02-RNAi, Super1300-Mi2G02-HA, Super1300-GT-3a-  
541 GFP and Super1300-GFP plasmids were used to transform *A. tumefaciens* strain  
542 GV3101. Four-week old *A. thaliana* plants were transformed with *A. tumefaciens* by  
543 the floral dip method (Clough and Bent, 1998). *A. thaliana* lines were confirmed to be  
544 homozygous for the transgene by qPCR and/or western blotting. Nematode infection  
545 assays were performed three times.

### 546 **Subcellular localization assay**

547 Four-week-old *N. benthamiana* leaves were infiltrated with *A. tumefaciens* carrying the  
548 appropriate plasmids in infiltration buffer (10 mM MgCl<sub>2</sub>, 10 mM MES, and 0.1 mM AS)  
549 at an OD<sub>600</sub> of 0.4. Images were captured by laser confocal fluorescence microscopy  
550 (Zeiss LSM700, Germany) 2 dpi, at an excitation wavelength of 488 nm for GFP and  
551 561 nm for mcherry.

### 552 **Yeast two-hybrid (Y2H) and yeast one-hybrid (Y1H) assays**

553 A cDNA library was constructed by extracting RNA from *A. thaliana* roots infected with  
554 *M. incognita* (1 dpi, 3 dpi, 5 dpi, 10 dpi, 14 dpi) and using it to screen for the target  
555 proteins of Mi2G02. The Y2H assay was performed according to the Clontech protocol  
556 (Clontech, USA). Interactions between Mi2G02 and candidate proteins were assessed  
557 in pairwise Y2H assays. Relative BD and AD vectors were used to transform the yeast  
558 strain Y2HGold for screening on SD/-Leu-Trp plates. Positive clones were verified and  
559 selected for culture on SD/-Leu-Trp-His medium supplemented with 20 mg/mL 5-  
560 bromo-4-chloro-3-indolyl- $\alpha$ -D-galactopyranoside (X- $\alpha$ -Gal; Coolaber, Cat. No.  
561 SL0940). We investigated the requirement of the nuclear localization sequences of  
562 *Mi2G02* for interaction by inserting a mutated *Mi2G02* in the BD vector for pairwise  
563 Y2H assays.

564 The Y1H assay was performed as previous described (Kong et al., 2023). The  
565 sequenced pB42AD and pLacZi vectors were integrated into the yeast strain EGY48  
566 grown on the SD/-Trp-Ura medium (Coolaber, Cat. No. PM2262). Positive  
567 transformants were verified and selected for growth on medium containing raffinose  
568 (Coolaber, Cat. No. SL0990), and 5-bromo-4-chloro-3-indolyl-b-D-galactopyranoside  
569 (X-gal, Coolaber, Cat. No. CX11921) for color reactions.

#### 570 **Bimolecular fluorescence complementation (BiFC) assay**

571 BiFC assays were performed as previously described (Zhao et al., 2019).  
572 *Agrobacterium* harboring appropriate pairs of vectors was infiltrated into *N.*  
573 *benthamiana* leaves for 48 h. YFP fluorescence, indicating protein interaction, was  
574 captured with a confocal microscope (Zeiss LSM700, Germany) with excitation at 514  
575 nm and emission at 527 nm.

#### 576 **Luciferase complementation assay**

577 *Agrobacterium* cultures were resuspended in infiltration buffer, incubated at room  
578 temperature for 3 h, and then infiltrated into four-week old *N. benthamiana* leaves.  
579 Three days after agro-infiltration, 1 mM luciferin (Biovision, Cat. No. 7903) solution  
580 was sprayed onto the infiltrated leaves, and luciferase activity was detected with a low-  
581 light cooled CCD imaging apparatus ChemiScope 6000 (Clinx Science Instruments  
582 Co., Ltd, Shanghai, China).

#### 583 **In vivo co-immunoprecipitation (Co-IP) assay**

584 Total protein was extracted from four-week-old *N. benthamiana* leaves co-expressing  
585 Mi2G02 and GT-3a, after 48 h of infiltration. Co-IP was performed with BeyoMag™  
586 Anti-HA Magnetic Beads (Beyotime, Cat. No. P2121) as previously described (Zhao  
587 et al., 2021). The eluted proteins were checked by western blotting with anti-GFP  
588 (ABclonal, Cat. No. AE012) and anti-HA (Coolaber, Cat. No. AB1105) antibodies,  
589 respectively.

#### 590 **Histochemical analysis of GUS activities**

591 Transgenic *A. thaliana* was generated as described above. The homozygosity of the  
592 transgenic lines was confirmed by PCR and they were inoculated with *M. incognita*.  
593 Root samples were collected at 3 dpi, 5 dpi, 7 dpi, and 14 dpi. More than 10 roots were  
594 collected at each sampling time. Histochemical staining for GUS enzyme activity was  
595 performed with a GUS staining kit (Coolaber, Cat. No. SL7160), in accordance with  
596 the manufacturer's instructions. Images were captured with a stereomicroscope (Zeiss,  
597 Axiolmager Z2, Germany).

**598 Dual-luciferase reporter assay**

599 *Agrobacterium* harboring pCAMBIA3301-GT-3a was infiltrated with *TOZpro-LUC-35S-*  
600 *Rluc* or *RAD23Cpro-LUC-35S-Rluc*, with or without Mi2G02, into four-week-old *N.*  
601 *benthamiana* leaves. Three days after infiltration, leaf discs with a diameter of 2 cm  
602 were harvested and ground in liquid nitrogen. Firefly and Renilla luciferase activities  
603 were measured with a Dual-Luciferase Reporter Assay System (Vazyme, Cat. No.  
604 DL101-01) according to the manufacturer's instructions, with Synergy SLXFA (BioTek,  
605 USA).

**606 Electrophoretic mobility shift assay (EMSA)**

607 The recombinant GT-3a-His protein was induced with 1 mM isopropyl- $\beta$ -d-  
608 thiogalactoside (IPTG) and purified with the His-tag Protein Purification Kit (Beyotime,  
609 Cat. No. P2229S) according to the manufacturer's instructions (Zhao et al., 2021). The  
610 biotin-labeled and unlabeled probes for *TOZ* and *RAD23C*, containing the -GTTAC-  
611 element or the -CACGTG- element, were synthesized and purified by Sangon Biotech  
612 (Shanghai, China). EMSA was carried out with an EMSA chemiluminescence kit  
613 (Beyotime, Cat. No. GS009). Competition experiments were performed with various  
614 amounts of unlabeled oligonucleotides. The mutated competitor was generated by  
615 replacing five base pairs or six base pairs in the *TOZ* and *RAD23C* binding elements  
616 (GTTAC to AAAAAA or CACGTG to AAAAAA). EMSA assays were repeated three  
617 times.

**618 Transient expression assays in *N. benthamiana* leaves**

619 Four-week-old *N. benthamiana* leaves were infiltrated with *A. tumefaciens* carrying the  
620 appropriate plasmids in infiltration buffer (10 mM MgCl<sub>2</sub>, 10 mM MES, and 0.1 mM AS)  
621 at an OD<sub>600</sub> of 0.4. MG132 (100  $\mu$ M) was added 24 h before protein extraction.

**622 Cell fractionation, protein extraction and western blotting**

623 Cell fractionation assay was followed as described previously (Wang et al., 2018) with  
624 some modifications. Briefly, *N. benthamiana* leaves expressing proper proteins (0.5 g)  
625 were harvested and ground in liquid nitrogen and mixed with 2 mL/g of lysis buffer (20  
626 mM Tris-HCl, pH 7.5, 20 mM KCl, 2 mM EDTA, 2.5 mM MgCl<sub>2</sub>, 25% glycerol, 250 mM  
627 sucrose, and 5mM DTT) supplemented with protease inhibitor cocktail (Beyotime, Cat.  
628 No. P1045). The homogenate was filtered through a double layer of Miracloth  
629 (Millipore, Cat. No. 475855). The flow-through was centrifuged at 1500g for 10 min at  
630 4°C, and the supernatant, consisting of the cytoplasmic fraction, was centrifuged at  
631 10,000g for 10 min at 4°C, and was collected as the cytoplasmic fraction. The pellet

632 from the first centrifugation was washed four times with 4 mL NRBT buffer (20 mM  
633 Tris-HCl, pH7.5, 2.5 mM MgCl<sub>2</sub>, 25% glycerol, and 0.2% TritonX-100) and then  
634 resuspended with 500 µL of NRB2 (20 mM Tris-HCl, pH 7.5, 10 mM MgCl<sub>2</sub>, 0.25 M  
635 sucrose, 0.5% Triton X-100, and 5 mM β-mercaptoethanol) supplemented with  
636 protease inhibitor cocktail and carefully overlaid on top of 500 µL of NRB3 (20 mM  
637 Tris-HCl, 10 mM MgCl<sub>2</sub>, pH 7.5, 1.7 M sucrose, 0.5% Triton X-100, and 5 mM β-  
638 mercaptoethanol) supplemented with protease inhibitor cocktail. The suspension was  
639 centrifuged at 16,000g for 45 min at 4°C, and the pellet was collected as the nuclear  
640 fraction. The 2× SDS loading buffer was then added to the cytoplasmic and nuclear  
641 fractions and boiled for 5 min. Actin was detected with an anti-actin antibody (ABclonal,  
642 Cat. No. AC009) as a cytoplasmic marker. H3 proteins were detected using an anti-  
643 H3 antibody (ABclonal, Cat. No. A2348) as a nuclear marker. Total proteins were  
644 extracted from *N. benthamiana* leaves or *A. thaliana* seedlings (ten days after  
645 germination) in RIPA lysis buffer (Beyotime, Cat. No. P0031K) supplemented with  
646 protease inhibitor cocktail. For tag antibodies, we used anti-His (TransGen, Cat. No.  
647 HT501), anti-GFP (ABclonal, Cat. No. AE012), and anti-HA (Coolaber, Cat. No.  
648 AB1105) antibodies, and a goat anti-mouse IgG (H+L)-HRP-conjugated secondary  
649 antibody (Coolaber, Cat. No. AB2102). The protein was detected with the EasySee  
650 Western Blot Kit (TransGen, Cat. No. DW101). Band intensity was determined by  
651 ImageJ software.

### 652 **Statistical methods**

653 The significance of differences between two groups was assessed in two-tailed *t*-tests.  
654 For multiple comparisons, the significance of differences was assessed by one-way  
655 ANOVA followed by Tukey tests for multiple comparisons. All statistical analyses were  
656 performed with GraphPad Prism software version 8.3.0.

### 657 **Accession numbers**

658 The accession numbers of major genes mentioned in this study are as follows: *Mi2G02*  
659 (*AAQ10016*), *GAPDH* (*Minc12412*), *GT-3a* (*AT5G01380*), *LBD41* (*AT3G02550*),  
660 *UBQ1* (*AT3G52590*), *TOZ* (*AT5G16750*), *RAD23C* (*AT3G02540*), *WRKY2*  
661 (*AT5G56270*), *UBP22* (*AT5G10790*), *SRP34* (*AT1G02840*), *DVL4* (*AT1G13245*),  
662 *SKP2* (*AT1G21410*), *FEI1* (*AT1G31420*), *FEI2* (*AT2G35620*), *ABS4* (*AT1G58340*).

### 663 **DATA AVAILABILITY**

664 All relevant data is included in the main manuscript and the Supplemental  
665 Information.

## 666 AUTHOR CONTRIBUTIONS

667 J.Z., B.F., P.A., M.Q., H.J. and Z.M. conceived the project. J.Z., K.H., B.F., Y.L., J.L.  
668 and Y.Y. designed and planned the experiments. J.Z., K.H., R.L., and Y.L. performed  
669 the experiments and collected and analyzed the data. J.Z., B.F., P.A. and M.Q. wrote  
670 the manuscript.

## 671 ACKNOWLEDGEMENTS

672 This research supported by the Youth Innovation Program of the Chinese Academy  
673 of Agricultural Sciences (Grant No. Y2022QC06), the National Natural Science  
674 Foundation of China (Grant Nos. 32001878, 32172366), the Natural Science  
675 Foundation of Beijing (Grant No. 6222054), the China Agriculture Research System  
676 (CARS-23), and the French Government (National Research Agency, ANR) through  
677 the 'Investments for the Future' LabEx SIGNALIFE (#ANR-11-LABX-0028-01), IDEX  
678 UCAJedi (#ANR-15-IDEX-0). We thank Dr Panpan Yang (Institute of Vegetables and  
679 Flowers, Chinese Academy of Agricultural Science, Beijing, China) for providing the  
680 CP516 vector and the p3301 vector, Dr Jinzhuo Jian (Institute of Plant Protection,  
681 Chinese Academy of Agricultural Science, Beijing, China) for advice concerning gall  
682 sections, and Dr Qian Wei (the Core Facility Platform, Institute of Crop Sciences,  
683 Chinese Academy of Agricultural Sciences, Beijing, China) for assistance with  
684 confocal microscopy.

## 685 COMPETING INTERESTS

686 The authors declare no competing interests.

## 687 REFERENCES

- 688 **Abad, P., Gouzy, J., Aury, J., Castagnone-Sereno, P., Danchin, E.G.J., Deleury,**  
689 **E., Perfus-Barbeoch, L., Anthouard, V., Artiguenave, F., and Blok, V.C., et al.**  
690 (2008). Genome sequence of the metazoan plant-parasitic nematode *Meloidogyne*  
691 *incognita*. *Nature Biotechnology* **26**:909-915. 10.1038/nbt.1482.
- 692 **Ayadi, M., Delaporte, V., Li, Y., and Zhou, D.** (2004). Analysis of GT-3a identifies a  
693 distinct subgroup of trihelix DNA-binding transcription factors in *Arabidopsis*. *FEBS*

- 694 *Letters* **562**:147-154. 10.1016/S0014-5793(04)00222-4.
- 695 **Baldacci-Cresp, F., Behr, M., Kohler, A., Badalato, N., Morreel, K., Goeminne, G.,**  
696 **Mol, A., de Almeida Engler, J., Boerjan, W., and El Jaziri, M., et al.** (2020).  
697 Molecular changes concomitant with vascular system development in mature galls  
698 induced by root-knot nematodes in the model tree host *Populus tremula* × *P. alba*.  
699 *International Journal of Molecular Sciences* **21**:406. 10.3390/ijms21020406.
- 700 **Barcala, M., García, A., Cabrera, J., Casson, S., Lindsey, K., Favery, B., García-**  
701 **Casado, G., Solano, R., Fenoll, C., and Escobar, C.** (2010). Early transcriptomic  
702 events in microdissected Arabidopsis nematode-induced giant cells. *Plant Journal*  
703 **61**:698-712. 10.1111/j.1365-313X.2009.04098.x.
- 704 **Bartlem, D.G., Jones, M.G.K., and Hammes, U.Z.** (2014). Vascularization and  
705 nutrient delivery at root-knot nematode feeding sites in host roots. *Journal of*  
706 *Experimental Botany* **65**:1789-1798. 10.1093/jxb/ert415.
- 707 **Cabrera, J., Barcala, M., Fenoll, C., and Escobar, C.** (2014). Transcriptomic  
708 signatures of transfer cells in early developing nematode feeding cells of  
709 Arabidopsis focused on auxin and ethylene signaling. *Frontiers in Plant Science*  
710 **5**:107. 10.3389/fpls.2014.00107.
- 711 **Cabrera, J., Díaz Manzano, F.E., Sanchez, M., Rosso, M.N., Melillo, T., Goh, T.,**  
712 **Fukaki, H., Cabello, S., Hofmann, J., and Fenoll, C., et al.** (2014). A role for  
713 *LATERAL ORGAN BOUNDARIES-DOMAIN 16* during the interaction *Arabidopsis-*  
714 *Meloidogyne* spp. provides a molecular link between lateral root and root-knot  
715 nematode feeding site development. *New Phytologist* **203**:632-645.  
716 10.1111/nph.12826.
- 717 **Caillaud, M., Dubreuil, G., Quentin, M., Perfus-Barbeoch, L., Lecomte, P., de**  
718 **Almeida Engler, J., Abad, P., Rosso, M., and Favery, B.** (2008). Root-knot  
719 nematodes manipulate plant cell functions during a compatible interaction. *Journal*  
720 *of Plant Physiology* **165**:104-113. 10.1016/j.jplph.2007.05.007.
- 721 **Chhabra, S., Chang, S.C., Nguyen, H.M., Huq, R., Tanner, M.R., Londono, L.M.,**  
722 **Estrada, R., Dhawan, V., Chauhan, S., and Upadhyay, S.K., et al.** (2014). Kv1.3  
723 channel-blocking immunomodulatory peptides from parasitic worms: implications for  
724 autoimmune diseases. *The FASEB Journal* **28**:3952-3964. 10.1096/fj.14-251967.
- 725 **Clough, S.J., and Bent, A.F.** (1998). Floral dip: a simplified method for  
726 *Agrobacterium*-mediated transformation of *Arabidopsis thaliana*. *Plant Journal*  
727 **16**:735-743. 10.1046/j.1365-313x.1998.00343.x.



- 728 **Dafny-Yelin, M., Chung, S., Frankman, E.L., and Tzfira, T.** (2007). pSAT RNA  
729 interference vectors: A modular series for multiple gene down-regulation in plants.  
730 *Plant Physiology* **145**:1272-1281. 10.1104/pp.107.106062.
- 731 **Eichmann, R., Richards, L., and Schäfer, P.** (2021). Hormones as go-betweeners in  
732 plant microbiome assembly. *Plant Journal* **105**:518-541. 10.1111/tpj.15135.
- 733 **Escobar, C., Brown, S., and Mitchum, M.G.** (2011) Transcriptomic and Proteomic  
734 Analysis of the Plant Response to Nematode Infection. In: Genomics and molecular  
735 genetics of plant-nematode interactions--Jones, J., Gheysen, G., and Fenoll, C.C.,  
736 ed.ed.s. Dordrecht: Springer Netherlands. 157-173. 10.1007/978-94-007-0434-3\_9.
- 737 **Farmer, L.M., Book, A.J., Lee, K., Lin, Y., Fu, H., and Vierstra, R.D.** (2010). The  
738 RAD23 family provides an essential connection between the 26S proteasome and  
739 ubiquitylated proteins in *Arabidopsis*. *The Plant Cell* **22**:124-142.  
740 10.1105/tpc.109.072660.
- 741 **Favery, B., Dubreuil, G., Chen, M., Giron, D., and Abad, P.** (2020). Gall-inducing  
742 parasites: Convergent and conserved strategies of plant manipulation by insects  
743 and nematodes. *Annual Review of Phytopathology* **58**:1-22. 10.1146/annurev-  
744 phyto-010820-012722.
- 745 **Favery, B., Lecomte, P., Gil, N., Bechtold, N., Bouchez, D., Dalmaso, A., and**  
746 **Abad, P.** (1998). RPE, a plant gene involved in early developmental steps of  
747 nematode feeding cells. *EMBO Journal* **17**:6799-6811. 10.1093/emboj/17.23.6799.
- 748 **Fuller, V.L., Lilley, C.J., Atkinson, H.J., and Urwin, P.E.** (2007). Differential gene  
749 expression in *Arabidopsis* following infection by plant-parasitic nematodes  
750 *Meloidogyne incognita* and *Heterodera schachtii*. *Molecular Plant Pathology* **8**:595-  
751 609. 10.1111/j.1364-3703.2007.00416.x.
- 752 **Gavrilovic, S., Yan, Z., Jurkiewicz, A.M., Stougaard, J., and Markmann, K.** (2016).  
753 Inoculation insensitive promoters for cell type enriched gene expression in legume  
754 roots and nodules. *Plant Methods* **12**:4. 10.1186/s13007-016-0105-y.
- 755 **Gheysen, G., and Mitchum, M.G.** (2019). Phytoparasitic nematode control of plant  
756 hormone pathways. *Plant Physiology* **179**:1212-1226. 10.1104/pp.18.01067.
- 757 **Griffith, M.E., Mayer, U., Capron, A., Ngo, Q.A., Surendrarao, A., McClinton, R.,**  
758 **Jürgens, G., and Sundaresan, V.** (2007). The *TORMOZ* gene encodes a nucleolar  
759 protein required for regulated division planes and embryo development in  
760 *Arabidopsis*. *The Plant Cell* **19**:2246-2263. 10.1105/tpc.106.042697.
- 761 **Guo, Q., Major, I.T., and Howe, G.A.** (2018). Resolution of growth-defense conflict:

- 762 mechanistic insights from jasmonate signaling. *Current Opinion in Plant Biology*  
763 **44**:72-81. 10.1016/j.pbi.2018.02.009.
- 764 **Hewezi, T., Juvale, P.S., Piya, S., Maier, T.R., Rambani, A., Rice, J.H., Mitchum,**  
765 **M.G., Davis, E.L., Hussey, R.S., and Baum, T.J.** (2015). The cyst nematode  
766 effector protein 10A07 targets and recruits host posttranslational machinery to  
767 mediate its nuclear trafficking and to promote parasitism in Arabidopsis. *The Plant*  
768 *Cell* **27**:891-907. 10.1105/tpc.114.135327.
- 769 **Hewitson, J.P., Ivens, A.C., Harcus, Y., Filbey, K.J., McSorley, H.J., Murray, J.,**  
770 **Bridgett, S., Ashford, D., Dowle, A.A., and Maizels, R.M.** (2013). Secretion of  
771 protective antigens by tissue-stage nematode larvae revealed by proteomic analysis  
772 and vaccination-induced sterile immunity. *Plos Pathogens* **9**:e1003492.  
773 10.1371/journal.ppat.1003492.
- 774 **Huang, G., Dong, R., Allen, R., Davis, E.L., Baum, T.J., and Hussey, R.S.** (2006).  
775 A root-knot nematode secretory peptide functions as a ligand for a plant transcription  
776 factor. *Molecular Plant-Microbe Interactions* **19**:463. 10.1094/MPMI-19-0463.
- 777 **Huang, G., Gao, B., Maier, T., Allen, R., Davis, E.L., Baum, T.J., and Hussey, R.S.**  
778 (2003). A profile of putative parasitism genes expressed in the esophageal gland  
779 cells of the root-knot nematode *Meloidogyne incognita*. *Molecular Plant-Microbe*  
780 *Interactions* **16**:376-381. 10.1094/MPMI.2003.16.5.376.
- 781 **Huot, B., Yao, J., Montgomery, B.L., and He, S.Y.** (2014). Growth-defense tradeoffs  
782 in plants: A balancing act to optimize fitness. *Molecular Plant* **7**:1267-1287.  
783 10.1093/mp/ssu049.
- 784 **Jammes, F., Lecomte, P., Almeida-Engler, J., Bitton, F., Martin-Magniette, M.,**  
785 **Renou, J.P., Abad, P., and Favery, B.** (2005). Genome-wide expression profiling  
786 of the host response to root-knot nematode infection in Arabidopsis. *Plant Journal*  
787 **44**:447-458. 10.1111/j.1365-313X.2005.02532.x.
- 788 **Jones, J.T., Haegeman, A., Danchin, E.G.J., Gaur, H.S., Helder, J., Jones, M.G.K.,**  
789 **Kikuchi, T., Manzanilla-López, R., Palomares-Rius, J.E., and Wesemael,**  
790 **W.M.L., et al.** (2013). Top 10 plant-parasitic nematodes in molecular plant  
791 pathology. *Molecular Plant Pathology* **14**:946-961. 10.1111/mpp.12057.
- 792 **Joshi, I., Kumar, A., Kohli, D., Bhattacharya, R., Sirohi, A., Chaudhury, A., and**  
793 **Jain, P.K.** (2022). Gall-specific promoter, an alternative to the constitutive  
794 *CaMV35S* promoter, drives host-derived RNA interference targeting *Mi-msp2* gene  
795 to confer effective nematode resistance. *Frontiers in Plant Science* **13**:1007322.

- 796 10.3389/fpls.2022.1007322.
- 797 **Joshi, I., Kumar, A., Singh, A.K., Kohli, D., Raman, K.V., Sirohi, A., Chaudhury,**  
798 **A., and Jain, P.K.** (2019). Development of nematode resistance in Arabidopsis by  
799 HD-RNAi-mediated silencing of the effector gene *Mi-msp2*. *Scientific Reports*  
800 **9**:17404. 10.1038/s41598-019-53485-8.
- 801 **Kang, M., Lee, S., Abdelmageed, H., Reichert, A., Lee, H.K., Fokar, M., Mysore,**  
802 **K.S., and Allen, R.D.** (2017). Arabidopsis stress associated protein 9 mediates  
803 biotic and abiotic stress responsive ABA signaling via the proteasome pathway.  
804 *Plant, Cell and Environment* **40**:702-716. 10.1111/pce.12892.
- 805 **Kaplan-Levy, R.N., Brewer, P.B., Quon, T., and Smyth, D.R.** (2012). The trihelix  
806 family of transcription factors-light, stress and development. *Trends in Plant Science*  
807 **17**:163-171. 10.1016/j.tplants.2011.12.002.
- 808 **Kong, D., Li, C., Xue, W., Wei, H., Ding, H., Hu, G., Zhang, X., Zhang, G., Zou, T.,**  
809 **and Xian, Y., et al.** (2023). UB2/UB3/TSH4-anchored transcriptional networks  
810 regulate early maize inflorescence development in response to simulated shade.  
811 *The Plant Cell* **35**:717-737. 10.1093/plcell/koac352.
- 812 **Lin, B., Zhuo, K., Wu, P., Cui, R., Zhang, L., and Liao, J.** (2013). A novel effector  
813 protein, MJ-NULG1a, targeted to giant cell nuclei plays a role in *Meloidogyne*  
814 *javanica* parasitism. *Molecular Plant-Microbe Interactions* **26**:55. 10.1094/MPMI-05-  
815 12-0114-FI.
- 816 **Liu, S., Yuan, X., Wang, Y., Wang, H., Wang, J., Shen, Z., Gao, Y., Cai, J., Li, D.,**  
817 **and Song, F.** (2019). Tomato stress-associated protein 4 contributes positively to  
818 immunity against necrotrophic fungus *Botrytis cinerea*. *Molecular Plant-Microbe*  
819 *Interactions* **32**:566-582. 10.1094/MPMI-04-18-0097-R.
- 820 **Livak, K.J., and Schmittgen, T.D.** (2001). Analysis of relative gene expression data  
821 using real-time quantitative PCR and the  $2^{-\Delta\Delta CT}$  method. *Methods* **25**:402-408.  
822 10.1006/meth.2001.1262.
- 823 **MacLean, A.M., Orlovskis, Z., Kowitwanich, K., Zdziarska, A.M., Angenent, G.C.,**  
824 **Immink, R.G.H., and Hogenhout, S.A.** (2014). Phytoplasma effector SAP54  
825 hijacks plant reproduction by degrading MADS-box proteins and promotes insect  
826 colonization in a RAD23-dependent manner. *Plos Biology* **12**:e1001835.  
827 10.1371/journal.pbio.1001835.
- 828 **Mejias, J., Bazin, J., Truong, N.M., Chen, Y., Marteu, N., Bouteiller, N., Sawa, S.,**  
829 **Crespi, M.D., Vaucheret, H., and Abad, P., et al.** (2021). The root-knot nematode

- 830 effector MiEFF18 interacts with the plant core spliceosomal protein SmD1 required  
831 for giant cell formation. *New Phytologist* **229**:3408-3423. 10.1111/nph.17089.
- 832 **Mejias, J., Chen, Y., Bazin, J., Truong, N., Mulet, K., Noureddine, Y., Jaubert-**  
833 **Possamai, S., Ranty-Roby, S., Soulé, S., and Abad, P., et al. (2022).** Silencing  
834 the conserved small nuclear ribonucleoprotein SmD1 target gene alters  
835 susceptibility to root-knot nematodes in plants. *Plant Physiology* **189**:1741-1756.  
836 10.1093/plphys/kiac155.
- 837 **Niu, J., Liu, P., Liu, Q., Chen, C., Guo, Q., Yin, J., Yang, G., and Jian, H. (2016).**  
838 Msp40 effector of root-knot nematode manipulates plant immunity to facilitate  
839 parasitism. *Scientific Reports* **6**:19443. 10.1038/srep19443.
- 840 **Nomura, K., Debroy, S., Lee, Y.H., Pumplin, N., Jones, J., and He, S.Y. (2006).** A  
841 bacterial virulence protein suppresses host innate immunity to cause plant disease.  
842 *Science* **313**:220-223. 10.1126/science.1129523.
- 843 **Olmo, R., Cabrera, J., Diaz-Manzano, F.E., Ruiz-Ferrer, V., Barcala, M., Ishida, T.,**  
844 **Garcia, A., Andres, M.F., Ruiz-Lara, S., and Verdugo, I., et al. (2020).** Root-knot  
845 nematodes induce gall formation by recruiting developmental pathways of post-  
846 embryonic organogenesis and regeneration to promote transient pluripotency. *New*  
847 *Phytologist* **227**:200-215. 10.1111/nph.16521.
- 848 **Olmo, R., Cabrera, J., Fenoll, C., and Escobar, C. (2019).** A role for *ALF4* during  
849 gall and giant cell development in the biotic interaction between *Arabidopsis* and  
850 *Meloidogyne* spp. *Physiologia Plantarum* **165**:17-28. 10.1111/ppl.12734.
- 851 **Olmo, R., Cabrera, J., Moreno-Risueno, M.A., Fukaki, H., Fenoll, C., and Escobar,**  
852 **C. (2017).** Molecular transducers from roots are triggered in *Arabidopsis* leaves by  
853 root-knot nematodes for successful feeding site formation: A conserved post-  
854 embryogenic *De novo* organogenesis program? *Frontiers in Plant Science* **8**:875.  
855 10.3389/fpls.2017.00875.
- 856 **Park, H.C., Kim, M.L., Kang, Y.H., Jeon, J.M., Yoo, J.H., Kim, M.C., Park, C.Y.,**  
857 **Jeong, J.C., Moon, B.C., and Lee, J.H., et al. (2004).** Pathogen- and NaCl-induced  
858 expression of the S<sub>CaM</sub>-4 promoter is mediated in part by a GT-1 Box that interacts  
859 with a GT-1-like transcription factor. *Plant Physiology* **135**:2150-2161.  
860 10.1104/pp.104.041442.
- 861 **Pieterse, C.M.J., Pierik, R., and Van Wees, S.C.M. (2014).** Different shades of JAZ  
862 during plant growth and defense. *New Phytologist* **204**:261-264.  
863 10.1111/nph.13029.

- 864 **Portillo, M., Lindsey, K., Casson, S., García-Casado, G., Solano, R., Fenoll, C.,**  
865 **and Escobar, C.** (2009). Isolation of RNA from laser-capture-microdissected giant  
866 cells at early differentiation stages suitable for differential transcriptome analysis.  
867 *Molecular Plant Pathology* **10**:523-535. 10.1111/j.1364-3703.2009.00552.x.
- 868 **Przybylska, A., and Szychalski, M.** (2021). Changes in the expression level of genes  
869 encoding transcription factors and cell wall-related proteins during *Meloidogyne*  
870 *arenaria* infection of maize (*Zea mays*). *Molecular Biology Reports* **48**:6779-6786.  
871 10.1007/s11033-021-06677-3.
- 872 **Qi, F., and Zhang, F.** (2020). Cell cycle regulation in the plant response to stress.  
873 *Frontiers in Plant Science* **10**:1765. 10.3389/fpls.2019.01765.
- 874 **Reitz, M.U., Gifford, M.L., and Schäfer, P.** (2015). Hormone activities and the cell  
875 cycle machinery in immunity-triggered growth inhibition. *Journal of Experimental*  
876 *Botany* **66**:2187-2197. 10.1093/jxb/erv106.
- 877 **Rich-Griffin, C., Eichmann, R., Reitz, M.U., Hermann, S., Woolley-Allen, K.,**  
878 **Brown, P.E., Wiwatdirekkul, K., Esteban, E., Pasha, A., and Kogel, K., et al.**  
879 (2020). Regulation of cell type-specific immunity networks in Arabidopsis roots. *The*  
880 *Plant Cell* **32**:2742-2762. 10.1105/tpc.20.00154.
- 881 **Sato, K., Uehara, T., Holbein, J., Sasaki-Sekimoto, Y., Gan, P., Bino, T.,**  
882 **Yamaguchi, K., Ichihashi, Y., Maki, N., and Shigenobu, S., et al.** (2021).  
883 Transcriptomic analysis of resistant and susceptible responses in a new model root-  
884 knot nematode infection system using *Solanum torvum* and *Meloidogyne arenaria*.  
885 *Frontiers in Plant Science* **12**:680151. 10.3389/fpls.2021.680151.
- 886 **Schiessl, K., Lilley, J.L.S., Lee, T., Tamvakis, I., Kohlen, W., Bailey, P.C., Thomas,**  
887 **A., Luptak, J., Ramakrishnan, K., and Carpenter, M.D., et al.** (2019). *NODULE*  
888 *INCEPTION* recruits the lateral root developmental program for symbiotic nodule  
889 organogenesis in *Medicago truncatula*. *Current Biology* **29**:3657-3668.  
890 10.1016/j.cub.2019.09.005.
- 891 **Schindelin, J., Arganda-Carreras, I., Frise, E., Kaynig, V., Longair, M., Pietzsch,**  
892 **T., Preibisch, S., Rueden, C., Saalfeld, S., and Schmid, B., et al.** (2012). Fiji: an  
893 open-source platform for biological-image analysis. *Nature Methods* **9**:676-682.  
894 10.1038/nmeth.2019.
- 895 **Shukla, N., Yadav, R., Kaur, P., Rasmussen, S., Goel, S., Agarwal, M., Jagannath,**  
896 **A., Gupta, R., and Kumar, A.** (2018). Transcriptome analysis of root-knot  
897 nematode (*Meloidogyne incognita*)-infected tomato (*Solanum lycopersicum*) roots

- 898 reveals complex gene expression profiles and metabolic networks of both host and  
899 nematode during susceptible and resistance responses. *Molecular Plant Pathology*  
900 **19**:615-633. 10.1111/mpp.12547.
- 901 **Song, H., Lin, B., Huang, Q., Sun, T., Wang, W., Liao, J., and Zhuo, K.** (2021). The  
902 *Meloidogyne javanica* effector Mj2G02 interferes with jasmonic acid signalling to  
903 suppress cell death and promote parasitism in *Arabidopsis*. *Molecular Plant*  
904 *Pathology* **22**:1288-1301. 10.1111/mpp.13111.
- 905 **Soyano, T., Shimoda, Y., Kawaguchi, M., and Hayashi, M.** (2019). A shared gene  
906 drives lateral root development and root nodule symbiosis pathways in *Lotus*.  
907 *Science* **366**:1021-1023. 10.1126/science.aax2153.
- 908 **Strader, L., Weijers, D., and Wagner, D.** (2022). Plant transcription factors-being in  
909 the right place with the right company. *Current Opinion in Plant Biology* **65**:102136.  
910 10.1016/j.pbi.2021.102136.
- 911 **Suzuki, R., Kanno, Y., Abril-Urias, P., Seo, M., Escobar, C., Tsai, A.Y., and Sawa,**  
912 **S.** (2022). Local auxin synthesis mediated by YUCCA4 induced during root-knot  
913 nematode infection positively regulates gall growth and nematode development.  
914 *Frontiers in Plant Science* **13**:1019427. 10.3389/fpls.2022.1019427.
- 915 **Suzuki, R., Yamada, M., Higaki, T., Aida, M., Kubo, M., Tsai, A.Y., and Sawa, S.**  
916 (2021). *PUCHI* regulates giant cell morphology during root-knot nematode infection  
917 in *Arabidopsis thaliana*. *Frontiers in Plant Science* **12**:755610.  
918 10.3389/fpls.2021.755610.
- 919 **Thein, M.C., Winter, A.D., Stepek, G., McCormack, G., Stapleton, G., Johnstone,**  
920 **I.L., and Page, A.P.** (2009). Combined extracellular matrix cross-linking activity of  
921 the peroxidase MLT-7 and the dual oxidase BLI-3 is critical for post-embryonic  
922 viability in *Caenorhabditis elegans*. *Journal of Biological Chemistry* **284**:17549-  
923 17563. 10.1074/jbc.M900831200.
- 924 **Tian, F., Yang, D., Meng, Y., Jin, J., and Gao, G.** (2019). PlantRegMap: charting  
925 functional regulatory maps in plants. *Nucleic Acids Research* **48**:D1104-D1113.  
926 10.1093/nar/gkz1020.
- 927 **Torres-Martínez, H.H., Rodríguez-Alonso, G., Shishkova, S., and Dubrovsky, J.G.**  
928 (2019). Lateral root primordium morphogenesis in angiosperms. *Frontiers in Plant*  
929 *Science* **10**:206. 10.3389/fpls.2019.00206.
- 930 **Tudor, J.E., Pallaghy, P.K., Pennington, M.W., and Norton, R.S.** (1996). Solution  
931 structure of ShK toxin, a novel potassium channel inhibitor from a sea anemone.

- 932 *Nature Structural Biology* **3**:317-320. 10.1038/nsb0496-317.
- 933 **Üstüner, S., Schäfer, P., and Eichmann, R.** (2022). Development specifies,  
934 diversifies and empowers root immunity. *EMBO Reports* **23**.  
935 10.15252/embr.202255631.
- 936 **Waese, J., Fan, J., Pasha, A., Yu, H., Fucile, G., Shi, R., Cumming, M., Kelley,**  
937 **L.A., Sternberg, M.J., and Krishnakumar, V., et al.** (2017). ePlant: Visualizing and  
938 exploring multiple levels of data for hypothesis generation in plant biology. *The Plant*  
939 *Cell* **29**:1806-1821. 10.1105/tpc.17.00073.
- 940 **Walter, M., Chaban, C., Schütze, K., Batistic, O., Weckermann, K., Näke, C.,**  
941 **Blazevic, D., Grefen, C., Schumacher, K., and Oecking, C., et al.** (2004).  
942 Visualization of protein interactions in living plant cells using bimolecular  
943 fluorescence complementation. *Plant Journal* **40**:428-438. 10.1111/j.1365-  
944 313X.2004.02219.x.
- 945 **Wang, K., He, J., Zhao, Y., Wu, T., Zhou, X., Ding, Y., Kong, L., Wang, X., Wang,**  
946 **Y., and Li, J., et al.** (2018). EAR1 Negatively Regulates ABA Signaling by  
947 Enhancing 2C Protein Phosphatase Activity. *The Plant Cell* **30**:815-834.  
948 10.1105/tpc.17.00875.
- 949 **Warmerdam, S., Sterken, M.G., van Schaik, C., Oortwijn, M.E.P., Sukarta, O.C.A.,**  
950 **Lozano-Torres, J.L., Dicke, M., Helder, J., Kammenga, J.E., and Goverse, A.,**  
951 **et al.** (2018). Genome-wide association mapping of the architecture of susceptibility  
952 to the root-knot nematode *Meloidogyne incognita* in *Arabidopsis thaliana*. *New*  
953 *Phytologist* **218**:724-737. 10.1111/nph.15034.
- 954 **Yamaguchi, Y.L., Suzuki, R., Cabrera, J., Nakagami, S., Sagara, T., Ejima, C.,**  
955 **Sano, R., Aoki, Y., Olmo, R., and Kurata, T., et al.** (2017). Root-knot and cyst  
956 nematodes activate procambium-associated genes in *Arabidopsis* roots. *Frontiers*  
957 *in Plant Science* **8**:1195. 10.3389/fpls.2017.01195.
- 958 **Zhang, L., Davies, L.J., and Elling, A.A.** (2015). A *Meloidogyne incognita* effector is  
959 imported into the nucleus and exhibits transcriptional activation activity *in planta*.  
960 *Molecular Plant Pathology* **16**:48-60. 10.1111/mpp.12160.
- 961 **Zhang, Q., Zhong, T., E, L., Xu, M., Dai, W., Sun, S., and Ye, J.** (2021). GT factor  
962 ZmGT-3b is associated with regulation of photosynthesis and defense response to  
963 *Fusarium graminearum* infection in maize seedling. *Frontiers in Plant Science*  
964 **12**:724133. 10.3389/fpls.2021.724133.
- 965 **Zhao, J., Li, L., Liu, Q., Liu, P., Li, S., Yang, D., Chen, Y., Pagnotta, S., Favery, B.,**

- 966 **and Abad, P., et al.** (2019). A MIF-like effector suppresses plant immunity and  
967 facilitates nematode parasitism by interacting with plant annexins. *Journal of*  
968 *Experimental Botany* **70**:5943-5958. 10.1093/jxb/erz348.
- 969 **Zhao, J., Sun, Q., Quentin, M., Ling, J., Abad, P., Zhang, X., Li, Y., Yang, Y.,**  
970 **Favery, B., and Mao, Z., et al.** (2021). A *Meloidogyne incognita* C-type lectin  
971 effector targets plant catalases to promote parasitism. *New Phytologist* **232**:2124-  
972 2137. 10.1111/nph.17690.
- 973 **Zhu, Y., Yuan, G., Zhao, R., An, G., Li, W., Si, W., Liu, J., and Sun, D.** (2022).  
974 Comparative transcriptome analysis reveals differential gene expression in resistant  
975 and susceptible watermelon varieties in response to *Meloidogyne incognita*. *Life*  
976 **12**:1003. 10.3390/life12071003.

977



978 **FIGURE LEGENDS**979 **Figure 1. Structure and nuclear localization of *M. incognita* effector Mi2G02.** (A)

980 Schematic diagram of the Mi2G02 and mutant Mi2G02 proteins. (B) Subcellular  
 981 localization of Mi2G02 and mutant Mi2G02 in plant cells. Coding sequences were  
 982 constructed into *ProSuper*:GFP (C-terminus GFP) vector. Mi2G02 and nuclear  
 983 localization signal mutants fused with GFP (Mi2G02-GFP, Mi2G02-mu1-GFP,  
 984 Mi2G02-mu2-GFP and Mi2G02-mu3-GFP) were co-expressed with mcherry in  
 985 *Nicotiana benthamiana* leaf cells. Empty vectors were used as controls. The  
 986 fluorescence signal was detected at 48 hours after infiltration. Mi2G02-GFP localized  
 987 to the nucleus. Mi2G02-mu1-GFP, Mi2G02-mu2-GFP and Mi2G02-mu3-GFP  
 988 primarily localized to the plasma membrane and cytoplasm. Images were captured  
 989 by confocal microscopy (Zeiss LSM 700, Germany). GFP, green fluorescent protein.  
 990 Scale bars, 20  $\mu$ m. (C) The relative abundance of Mi2G02-GFP or Mi2G02-mu-GFP  
 991 in cytoplasmic and nuclear fractions was detected using anti-GFP antibodies after  
 992 transiently expressing in *N. benthamiana* leaf cells. Actin was used as an internal  
 993 reference for the presence of cytoplasmic proteins and Histone H3 was used as an  
 994 internal reference for the presence of nuclear proteins.

995 **Figure 2. Host-derived RNA interference (RNAi) and ectopic expression of**  
 996 ***Mi2G02* in *A. thaliana* alter plants susceptibility to *M. incognita* and root**  
 997 **development.** (A) *Mi2G02* expression level in three homozygous RNAi lines

998 (Mi2G02-Ri-1, Mi2G02-Ri-2 and Mi2G02-Ri-4), gfp-RNAi line (GFP-Ri) and wild type  
 999 (WT) were determined at 10 days post infection (dpi) of *M. incognita* by RT-qPCR.  
 1000 *GAPDH* was used as an internal control. The values shown are means  $\pm$  SE (n = 3).  
 1001 Different letters indicate significant differences ( $P < 0.05$ , one-way ANOVA). (B) Gall  
 1002 numbers and egg mass numbers per plant at 35 dpi. Values are presented as means  
 1003  $\pm$  SD (n=18). Different letters indicate significant differences ( $P < 0.05$ , one-way  
 1004 ANOVA). See also Figure S1B. (C) Giant cell areas of *M. incognita*-induced galls in  
 1005 the *A. thaliana* Mi2G02-Ri lines were significantly reduced. Gall sections at 14 days  
 1006 post infection (dpi) were stained with toluidine-blue. Relatively smaller giant cells  
 1007 were observed in Mi2G02-Ri mature galls at 14 dpi compared with the WT and GFP-  
 1008 Ri controls. Data are the average surface areas  $\pm$  SD (n=10) for each line. Different  
 1009 letters indicate significant differences ( $P < 0.05$ , one-way ANOVA). Asterisk, giant cell;  
 1010 N, nematode. Bars, 100  $\mu$ m. (D) *A. thaliana* phenotypes and relative root length of

1011 *Mi2G02* ectopic expressing *A. thaliana* lines compared with wild-type. Data  
1012 represents the average length  $\pm$  SD (n=10). Different letters indicate significant  
1013 differences ( $P<0.05$ , one-way ANOVA). Scale bar, 1 cm. See also Figure S2C. (E)  
1014 Expression of *Mi2G02* in *A. thaliana* increased susceptibility to *M. incognita*. Two  
1015 independent *Mi2G02*-T3 lines were inoculated with *M. incognita* pre-J2s. Total  
1016 numbers of galls and egg masses were counted at 35 dpi. *M. incognita* inoculated  
1017 wild-type *A. thaliana* plant was used as control. Data are the average numbers per  
1018 plant  $\pm$  SD (n=16). Different letters indicate significant differences ( $P<0.05$ , one-way  
1019 ANOVA). See also Figure S2D.

1020 **Figure 3. The *Mi2G02* effector interacts with *GT-3a* in the nuclei.** (A) Schematic  
1021 representation of the intact and truncated *Mi2G02* (with or without ShKT domain)  
1022 and *GT-3a* (with or without DNA binding domain) used for yeast two-hybrid assays  
1023 (Y2Hs). (B) Pairwise Y2H tests were performed to investigate the interactions  
1024 between *Mi2G02* or ShKT domains and *GT-3a* or DNA binding (DB) domain. Left  
1025 column, yeast cell growth carrying the baits in pGBKT7 vector (BD) and preys in  
1026 pGADT7 (AD) grown on SD/-Trp-Leu (SD-WL) medium indicating successful  
1027 transformation of the yeast with both plasmids; right column, yeast cell growth on the  
1028 selective dropout medium (SD/-Trp-Leu-His, SD-WLH) following the addition of 20  
1029 mg/ml X- $\alpha$ -gal indicating protein interaction. Yeast cells containing p53 and SV40  
1030 large T-antigen were used as positive control, and yeast cells containing Lamin and  
1031 SV40 large T-antigen were used as negative control. (C) Pairwise Y2H tests were  
1032 performed to investigate the interactions between *Mi2G02* mutants and *GT-3a*. (D)  
1033 *Mi2G02* colocalizes with *GT-3a* in *N. benthamiana* cell nuclei. *Mi2G02* fused with  
1034 GFP in C-terminus (*Mi2G02*-GFP) and *GT-3a* fused with mcherry in N-terminus  
1035 (mcherry-*GT-3a*) were co-expressed in *N. benthamiana* leaf cells. The fluorescence  
1036 signal was detected at 48 h after infiltration. Images were captured by confocal  
1037 microscopy. Scale bars, 20  $\mu$ m. (E) Bimolecular fluorescence complementation  
1038 (BiFC) experiments demonstrate the interaction between *Mi2G02* and *GT-3a*. *N.*  
1039 *benthamiana* leaves were transformed with different combinations of nEYFP and  
1040 cEYFP fused vectors. Images were obtained 48 h after co-expression. Yellow  
1041 fluorescent protein (YFP) fluorescence signals were observed in the nuclei in leaves  
1042 co-infiltrated with nEYFP-*Mi2G02* and *GT-3a*-cEYFP. Scale bars, 20  $\mu$ m. See also  
1043 Figure S3C. (F) Determination of the interaction between *Mi2G02* and *GT-3a*

1044 through luciferase complementation assay (LCA). *A. tumefaciens* harboring different  
 1045 combinations of plasmids were infiltrated into indicated regions of *N. benthamiana*  
 1046 leaves. The luciferase activities were recorded at 2 days post agro-infiltration by  
 1047 spraying 1 mM luciferin solution onto the infiltrated leaves, and the luciferase activity  
 1048 was detected with a low-light cooled CCD imaging apparatus. Luciferase activity was  
 1049 depicted with false color from low (black) to high (white). The protein levels of  
 1050 Mi2G02-NLuc, Mi2G02-mu1-NLuc, Mi2G02-mu2-NLuc, Mi2G02-mu3-NLuc, CLuc-  
 1051 GT-3a, GUS-NLuc, CLuc-GUS were determined by western blotting using anti-  
 1052 Luciferase antibody. Ponceau S (P) staining provided a loading control. (G) Mi2G02  
 1053 associates with GT-3a in a co-immunoprecipitation (Co-IP) assay. *A. tumefaciens*  
 1054 harboring different combinations of plasmids were infiltrated into *N. benthamiana*  
 1055 leaves. Co-IP was performed with BeyoMag™ Anti HA Magnetic Beads, and the  
 1056 eluted protein was detected using western blotting with antibody against HA and  
 1057 GFP. GFP, green fluorescent protein. P, ponceau staining indicates samples  
 1058 loading.

1059 **Figure 4. GT-3a is involved in *M. incognita* parasitism and lateral roots**  
 1060 **development.** (A) The activity of *GT-3a* promoter was analysed in uninfected roots  
 1061 and in galls induced by *M. incognita* in *A. thaliana* expressing the *ProGT-3a:GUS*  
 1062 construct. Scale bars, 100  $\mu$ m. dpi, days-post infection. (B) *A. thaliana* phenotypes,  
 1063 relative root length and relative lateral root numbers of *Mi2G02* ectopic expressing *A.*  
 1064 *thaliana* lines compared with wild-type. Data represents the average length  $\pm$  SD  
 1065 (n=10) and the average number  $\pm$  SD (n=10). Different letters indicate significant  
 1066 differences ( $P < 0.05$ , one-way ANOVA). Scale bar, 1 cm. See also Figure S4H. (C)  
 1067 Lateral root density calculated as the number of emerged lateral roots divided by  
 1068 total primary root length. Different letters indicate significant differences ( $P < 0.05$ ,  
 1069 one-way ANOVA). (D) Overexpression of *GT-3a* in *A. thaliana* increased  
 1070 susceptibility to *M. incognita*. Two independent *GT-3a* ectopic expressing T3 lines  
 1071 were inoculated with *M. incognita* pre-J2s. Total numbers of galls and egg masses  
 1072 were counted at 35 dpi. *M. incognita* inoculated wild-type *A. thaliana* plant was used  
 1073 as control. Data are the average number  $\pm$  SD (n=18). Different letters indicate  
 1074 significant differences ( $P < 0.05$ , one-way ANOVA). See also Figure S5A. (E) The *gt-*  
 1075 *3a* T-DNA knockout mutants (SALK\_134703 and SALK\_040448) were less  
 1076 susceptible to *M. incognita* compared with the wild-type, as indicated by the mean

1077 numbers of galls and egg masses. Data are the average number  $\pm$  SD (n=26).  
 1078 Different letters indicate significant differences ( $P<0.05$ , one-way ANOVA). See also  
 1079 Figure S5B. (F) Giant cell areas of *M. incognita*-induced galls in the *A. thaliana* *gt-3a*  
 1080 T-DNA knockout mutant lines were significantly reduced. Gall sections at 21 dpi  
 1081 were stained with toluidine-blue. Relatively smaller giant cells were observed in *gt-3a*  
 1082 T-DNA knockout mutant lines compared with the wild-type. Data are the average  
 1083 surface area  $\pm$  SD (n=10). Different letters indicate significant differences ( $P<0.05$ ,  
 1084 one-way ANOVA). Asterisk, giant cell; N, nematode. Bars, 100  $\mu$ m.

1085 **Figure 5. Targeting and suppression of *TOZ* and *RAD23C* by *GT-3a* and the**  
 1086 **susceptibility of *toz* and *rad23c* knockout mutant lines to *M. incognita*.** (A)  
 1087 Transcriptional activity of *GT-3a* in yeast cells. The yeast AH109 strain expressing  
 1088 pCL-1, *GT-3a*, *GT-3a* with or without DNA binding domain (*GT-3a-DB* or *GT-3a-*  
 1089  $\Delta$ *DB*) grew on Yeast Peptone Dextrose Adenine Agar (YPDA) or the selective  
 1090 medium SD-His-Trp with or without X- $\alpha$ -gal. The pCL-1 encoding the full-length  
 1091 GAL4 and the empty vector pGBKT7 (BD) were used as positive and negative  
 1092 controls, respectively. (B) Yeast one-hybrid (Y1H) experiments showed *GT-3a* bound  
 1093 to the promoter of *TOZ*, *RAD23C* and *WRKY2*. Promoter fragments containing -  
 1094 GTTAC- or -CACGTG- element were cloned into pLacZi vector, *GT-3a* was cloned  
 1095 into pB42AD vector, and then pLacZi vector co-transformed with pB42AD-*GT-3a* into  
 1096 yeast strain EGY48. The yeast transformants were spotted on the plate SD/-Ura-Trp  
 1097 with or without 20 mg/ml X-gal. pB42AD-p53 and pLacZi-p53 were used as a  
 1098 positive control. (C) Luciferase reporter assays of *GT-3a*-induced suppression of  
 1099 *TOZ* and *RAD23C* expression in *N. benthamiana*. LUC activity was measured by  
 1100 normalizing to REN signal. Values are means  $\pm$  SE (n = 4). Asterisks mark significant  
 1101 differences according to two-tailed Student's *t* test, \*\*\* $P<0.001$ . Similar results were  
 1102 obtained from three independent experiments (biological replicates). (D) qRT-PCR  
 1103 analysis of *TOZ* and *RAD23C* expression in wild type *A. thaliana* and *GT-3a*  
 1104 overexpressing *A. thaliana* lines. *UBP22* (*AT5G10790*) was used as an internal  
 1105 control. Data represent the mean of three independent experiments  $\pm$  SE (n=3).  
 1106 Similar results were obtained from three independent experiments (biological  
 1107 replicates). Different letters indicate significant differences ( $P<0.05$ , one-way  
 1108 ANOVA). (E) EMSA assays confirmed *GT-3a*-His could direct bind to the promoter of  
 1109 *TOZ* and *RAD23C*. Promoter fragments containing -GTTAC- element (P1 probe) or -

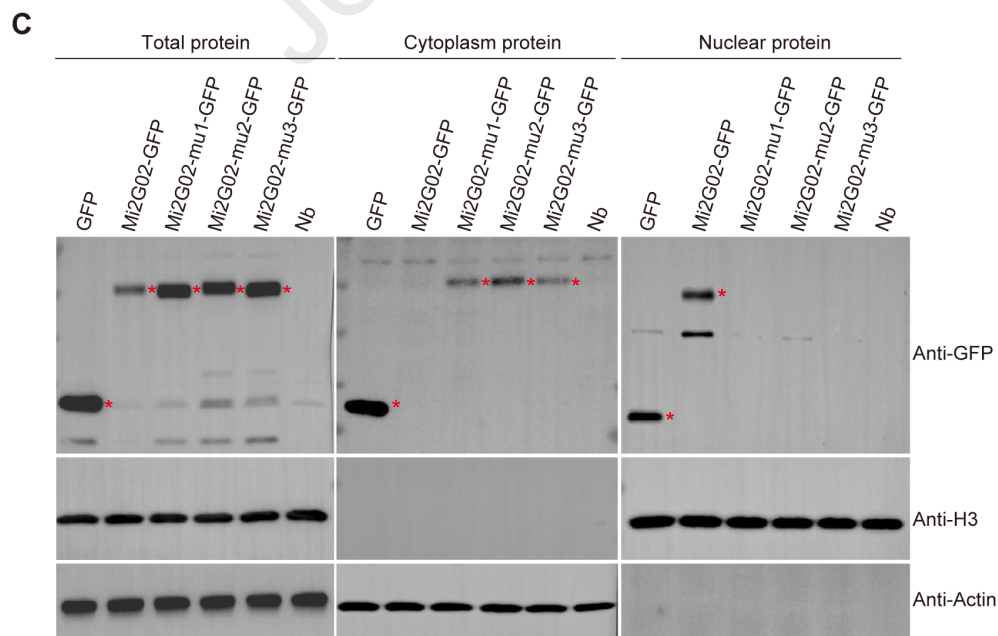
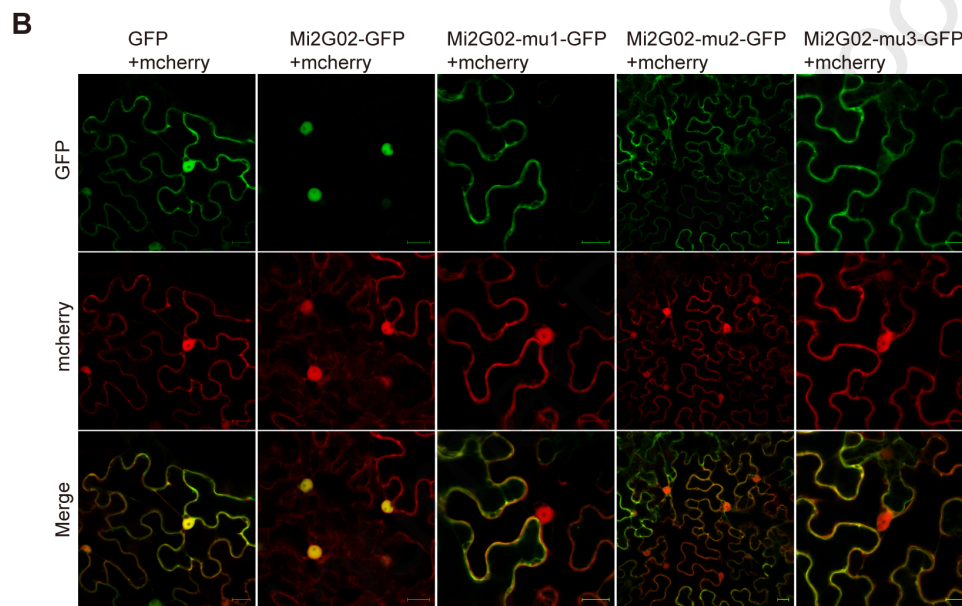
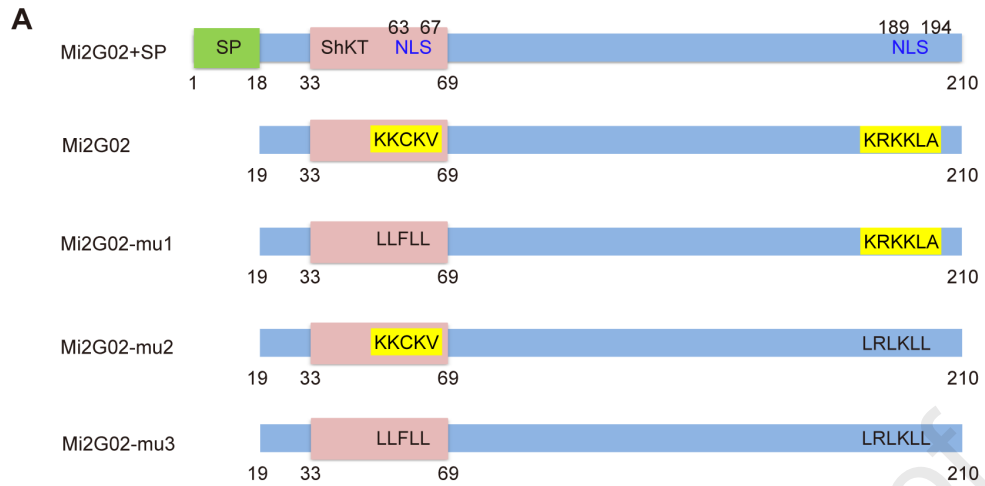
1110 CACGTG- element (P2 probe) or mutant elements (-AAAAA- or -AAAAAA-) were  
1111 labeled with biotin as probes. 6xHis alone served as a negative control. Unlabeled  
1112 probes were used as competing probes.

1113 **Figure 6. Mi2G02 stabilizes GT-3a to promote its function in suppression of**  
1114 **TOZ and RAD23C expression for nematode parasitism.** (A) The *rad23c* T-DNA  
1115 knockout mutant is more susceptible than the wild type to *M. incognita*. The *rad23c*  
1116 KO mutant (*SALK\_068091*) was inoculated with nematodes, and the numbers of  
1117 galls and egg masses were counted 35 days post-inoculation. The data presented  
1118 are the mean numbers per plant  $\pm$  SD ( $n=28$ ). Similar results were obtained in three  
1119 independent experiments. Asterisks indicate differences that were significant in two-  
1120 tailed Student's *t* tests,  $**P<0.01$ . See also Figure S7E. (B) Luciferase reporter  
1121 assays showed that the GT-3a-induced suppression of *TOZ* and *RAD23C*  
1122 expression in *N. benthamiana* was enhanced by Mi2G02 expression. LUC activity  
1123 was determined and normalized against the REN signal. The data presented are the  
1124 means of three independent experiments  $\pm$  SEM ( $n=4$ ). Different letters indicate  
1125 significant differences ( $P<0.05$ , one-way ANOVA). (C) Mi2G02 stabilizes the GT-3a-  
1126 GFP fluorescence intensity. *GT-3a* was co-expressed with *Mi2G02* in *N.*  
1127 *benthamiana* leaves, and Mi2G02 mutants and MiEFF18 (a nuclear *M. incognita*  
1128 effector not interacted with GT-3a) were used as controls. The GT-3a-GFP  
1129 fluorescence was detected with confocal microscopy (LSM700, Zeiss) 48 h after  
1130 infiltration. Graphs showed the fluorescence intensity profiles across the arrows in  
1131 the GFP images. Bar = 10  $\mu$ m. See also Figure S8. (D) Mi2G02 stabilizes the GT-3a  
1132 protein, leading to its accumulation. *GT-3a* was co-expressed with *Mi2G02* or *GFP* in  
1133 *N. benthamiana* leaves. The GT-3a protein was detected with an anti-GFP antibody.  
1134 Band intensity was determined with ImageJ software and is indicated below the  
1135 bands. CBB, Coomassie brilliant blue staining, and P, Ponceau staining, were used  
1136 to check protein sample loading. (E) Mi2G02 inhibits of the GT-3a degradation via  
1137 26S proteasome pathway *in vivo*. GT-3a-GFP was co-expressed with Mi2G02-HA  
1138 and Mi2G02 mutants in *N. benthamiana* leaves, respectively. The 26S proteasome  
1139 inhibitor MG132 (100  $\mu$ M) was infiltrated into *N. benthamiana* leaves 24 h before  
1140 protein extraction. Band intensity was determined by ImageJ software and is  
1141 indicated below the bands.

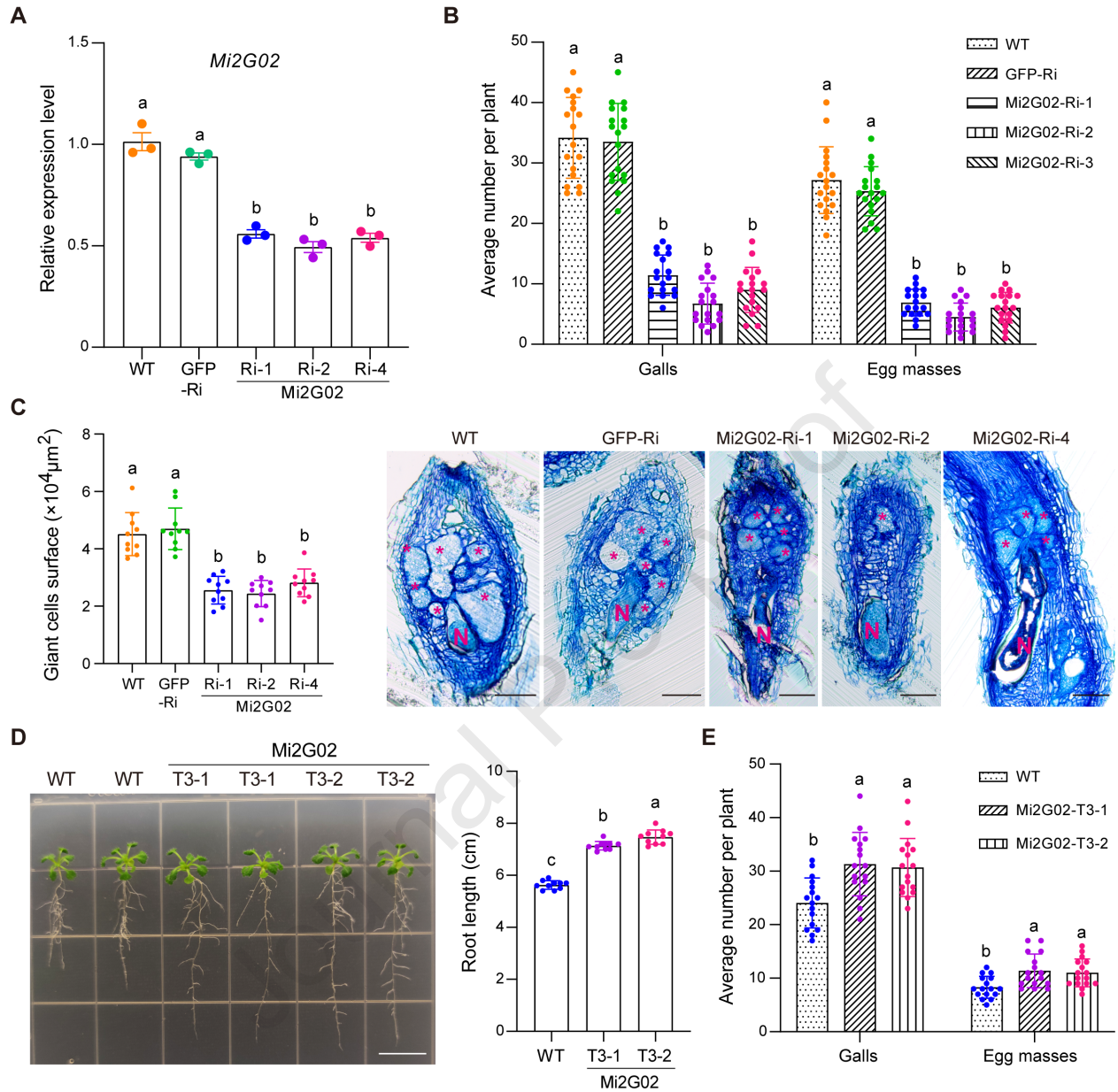
1142 **Figure 7 A proposed working model illustrating the molecular mechanism of**  
1143 **the interaction among Mi2G02, GT-3a and TOZ, RAD23C in the nematode**  
1144 **parasitism.** In the early stage of *M. incognita* parasitism, Mi2G02 effector protein is  
1145 secreted into the plant cell and translocates to the plant nucleus, where targets the  
1146 transcription factor GT-3a and stabilizes its proteins level by inhibiting 26S  
1147 proteasome pathway, leading to the suppression of TOZ and RAD23C expression  
1148 for nematode feeding cells formation and development.

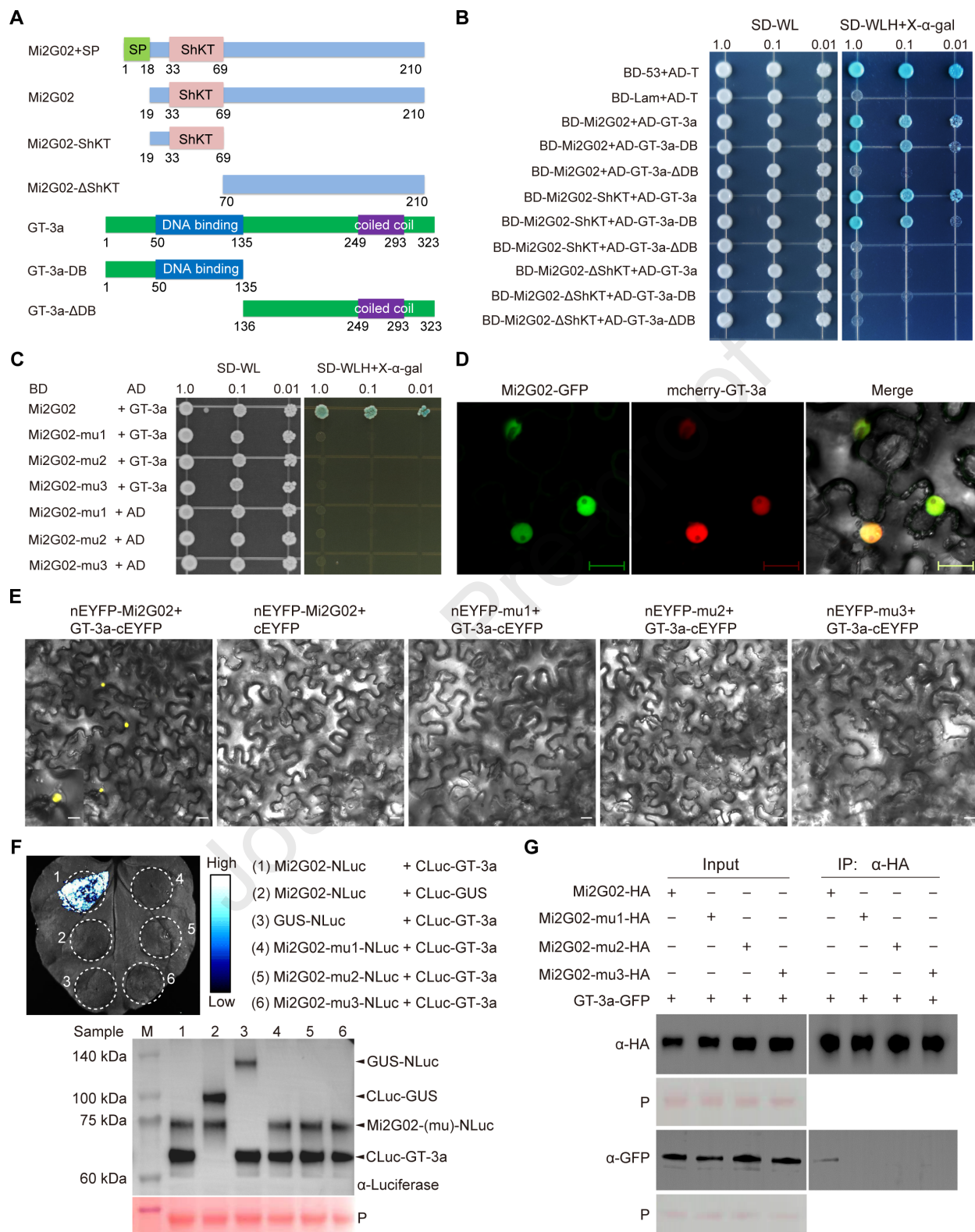
Journal Pre-proof

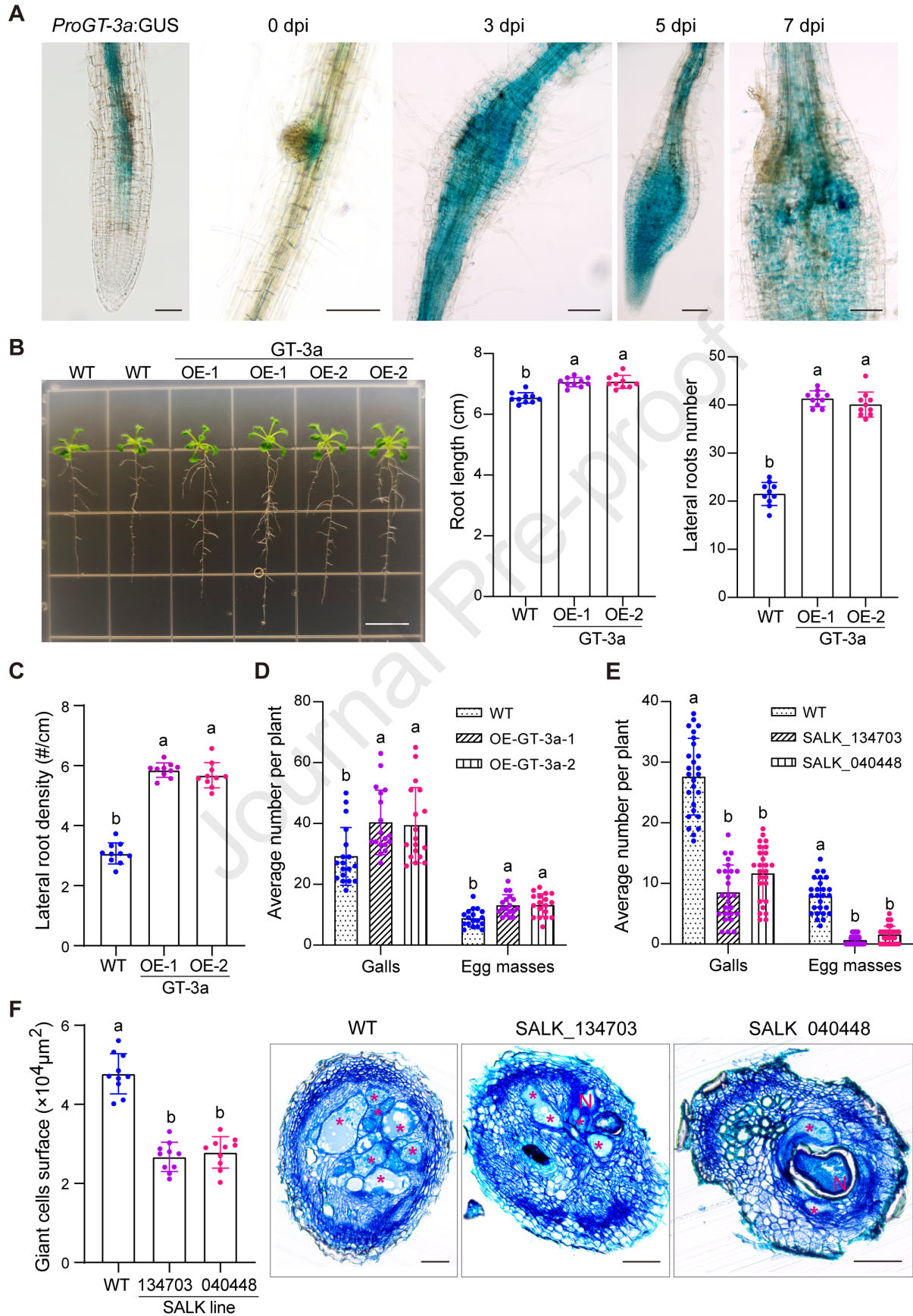
Journal Pre-proof

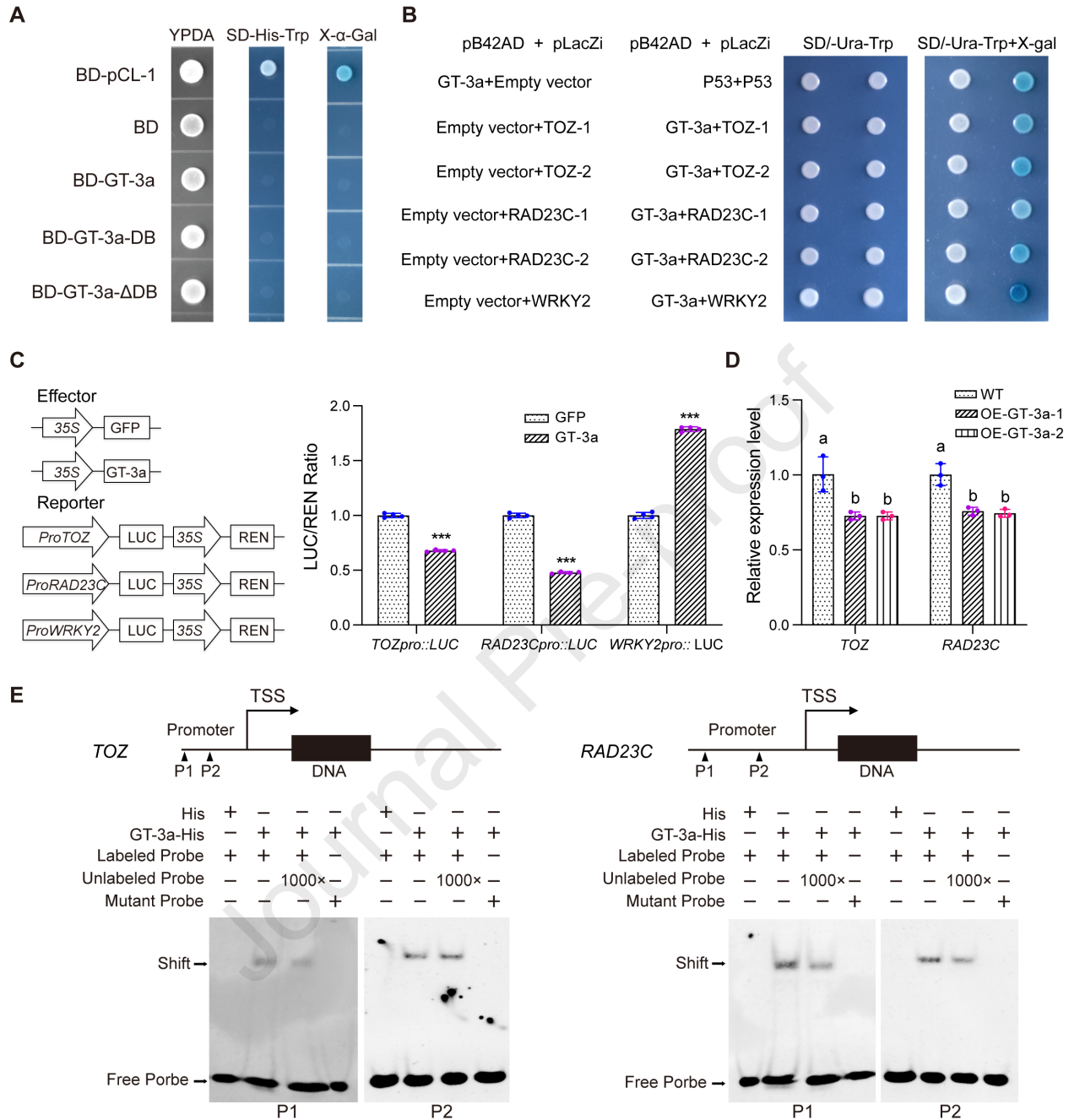


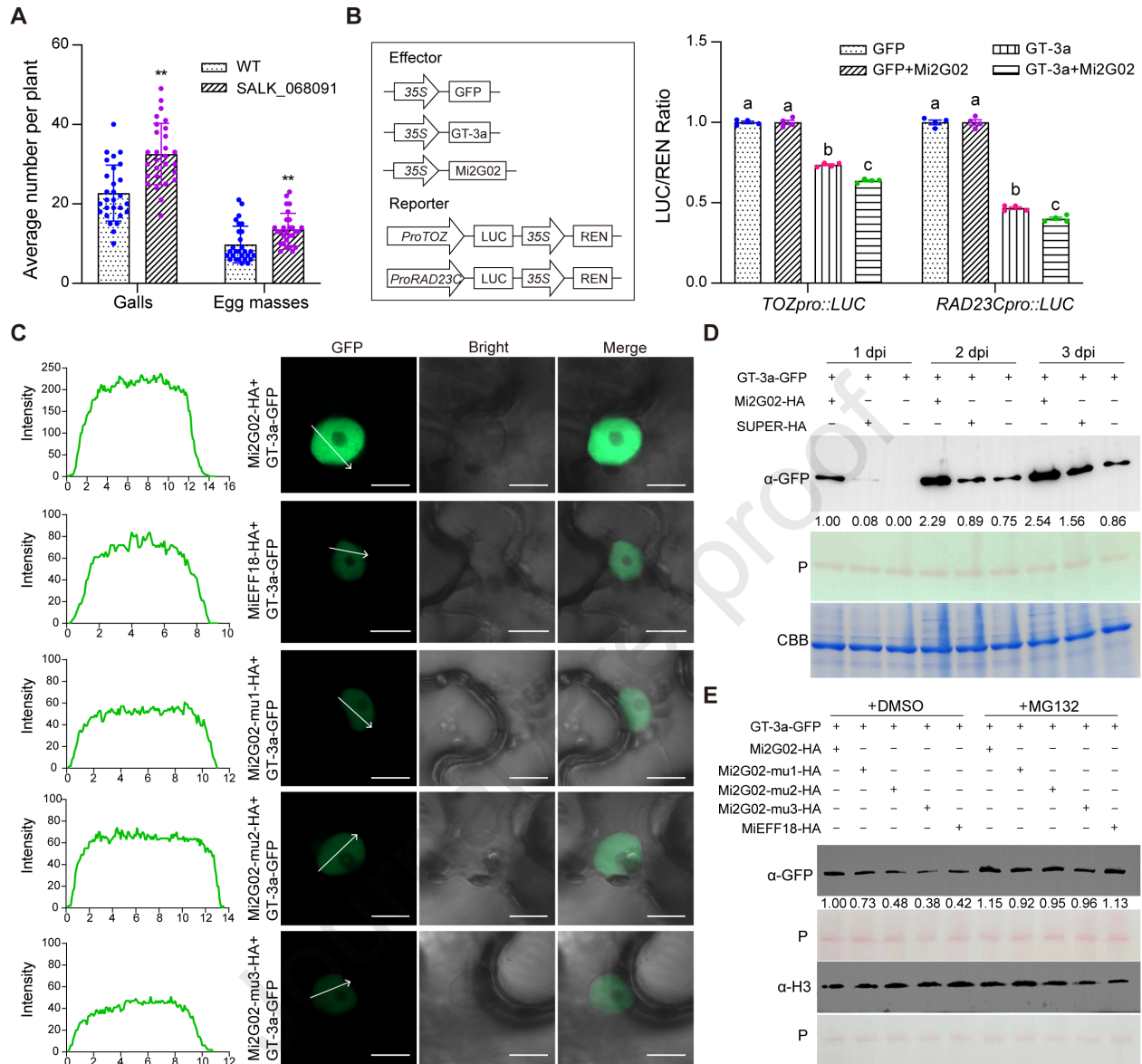


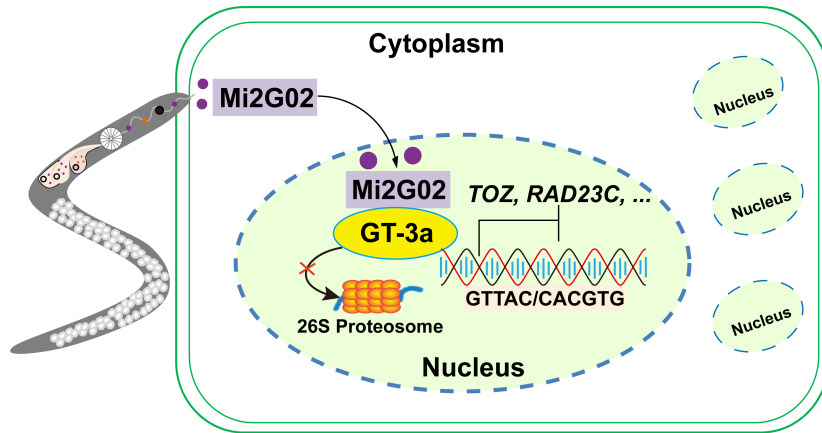












Journal Pre-proof